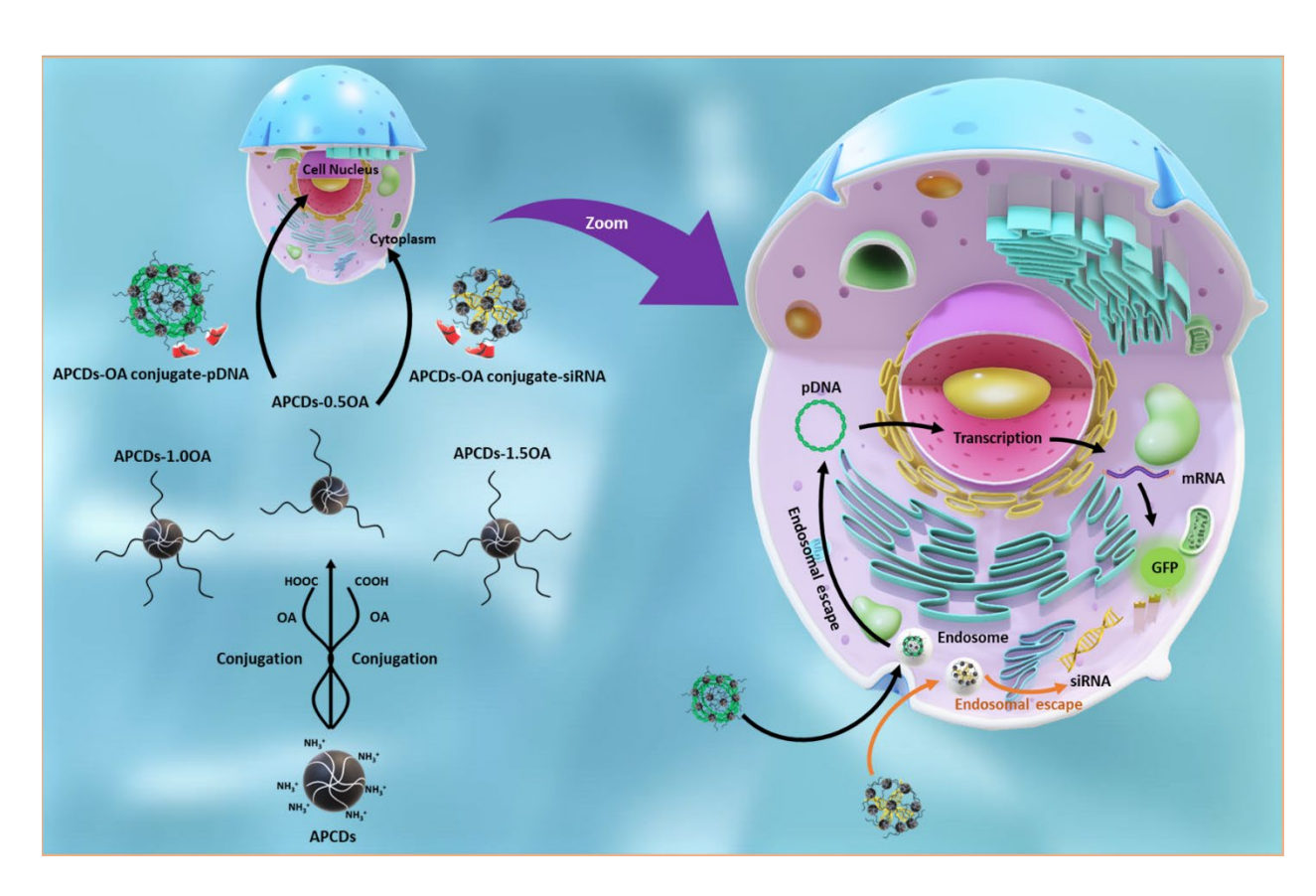
Gene transfection efficiency improvement with lipid conjugated

| 2 | cationic carbon dot |
|----|--|
| 3 | Jiuyan Chen, ^{1†} Fang Li, ^{2†} Bowen Zhao, ^{1†} Jun Gu, ³ Nicholas Michael Brejcha, ² Mattia Bartoli, ⁴ |
| 4 | Wei Zhang, ¹ Yiqun Zhou, ¹ Shiwei Fu, ¹ Justin B. Domena, ¹ Alyan Zafar, ² Fuwu Zhang, ¹ Alberto |
| 5 | Tagliaferro, ⁴ Fulvia Verde, ³ Fangliang Zhang, ³ Yanbin Zhang, ^{2*} Roger M. Leblanc ^{1*} |
| 6 | ¹ Department of Chemistry, University of Miami, Coral Gables, FL 33146, USA |
| 7 | ² Department of Biochemistry and Molecular Biology, Miller School of Medicine, University of Miami, |
| 8 | FL 33136, USA |
| 9 | ³ Department of Molecular and Cellular Pharmacology, Miller School of Medicine, University of Miami, |
| 10 | FL 33136, USA |
| 11 | ⁴ Department of Applied Science and Technology, Politecnico di Torino, 10129, Italy |
| 12 | |
| 13 | |
| 14 | |
| 15 | |
| 16 | |



Abstract

An ideal vehicle with high transfection efficiency is crucial for gene delivery. In this study, a type of cationic carbon dots (CCDs) that named APCDs were firstly prepared with arginine (Arg) and pentaethylenehexamine (PEHA) as precursors and conjugated with oleic acid (OA) for gene delivery. By tuning the mass ratio of APCDs to OA, APCDs-OA conjugates, namely APCDs-0.5OA, APCDs-1.0OA and APCDs-1.5OA were synthesized. All the three amphiphilic APCDs-OA conjugates show high affinity to DNA through electrostatic interactions. APCDs-0.5OA exhibit strong binding with small interfering RNA (siRNA). After being internalized by Human Embryonic Kidney (HEK 293) and osteosarcoma (U2OS) cells, they could distribute in both the cytoplasm and the nucleus. With APCDs-OA conjugates as gene delivery vehicles, the plasmid DNA (pDNA) that encodes the gene for the green fluorescence protein (GFP) can be successfully delivered into both HEK 293 and U2OS cells. The GFP expression level mediated by APCDs-0.5OA and APCDs-1.0OA are ten times higher than that of PEI in HEK 293 cells. Furthermore, APCDs-0.5OA show prominent siRNA transfection efficiency, which is proved by the significantly downregulated expression of FANCA and FANCD2 proteins upon delivery of FANCA siRNA and FANCD2 siRNA into U2OS cells. In conclusion, our work demonstrates that

conjugation of CCDs with lipid structure such as OA significantly improves the gene transfection efficiency, providing a new idea about the designation of non-viral carriers in gene delivery systems.

Keywords: cationic carbon dots, lipid, gene delivery, plasmid DNA, small interfering RNA

1. Introduction

Gene therapy, a strategy for treating diseases caused by genetic disorders such as cystic fibrosis, cancers, and Parkinson's diseases, has attracted tremendous attention in medical research. This pioneering approach relies on the introduction of external genetic materials such as plasmid DNA (pDNA), messenger RNA (mRNA) and small interfering RNA (siRNA) into living cells to achieve precise editing, replacement, or alteration of gene expression. However, the cell membrane penetration of nucleic acids is restricted by their negative charges and high molecular weight. Even the exogenous nucleic acids in the cells might be degraded in the endosome. ¹⁻⁴ In this regard, development of a promising carrier for the protection and efficient delivery of genetic materials into target cells is of immense importance in gene therapy. In general, gene delivery carriers can be divided into viral and non-viral vehicles. Viral vehicles are efficient for gene delivery. Nevertheless, obstacles that concern the ease of rapid clearance by pre-existing antibodies, the triggering host immunogenicity, the risk of genome mutation and potential side effects have been reported. These challenges have hindered their clinical applications. ^{5,6} To address these issues, significant research endeavors have been dedicated to the development of non-viral delivery systems.

The current studies of non-viral vehicles are focused on cationic polymers, cationic liposomes, and nanomaterials. ^{7, 8} The advantages including high transfection efficiency, negligible immunogenicity, and structural designability make them ideal substitutes for viral vehicles. ⁹ In addition to the commonly used lipid-nanoparticles and polymeric nanoparticles, which are prepared by assembling lipids or polymers (such as dextran, chitosan, cyclodextrins and synthetic polymers), gold nanoparticles, silica nanoparticles, magnetic nanoparticles, carbon nanotubes and carbon dots (CDs) are also widely investigated for gene delivery. ^{8, 10-13} CDs typically refer to a class of zero-dimensional carbon nanomaterials with particle sizes less than 10 nm. Considering their intrinsic properties encompassing low cytotoxicity, high water solubility, excellent biocompatibility, superior photostability, and easily functionalized surface, they have been

extensively applied in bioimaging, biosensing, drug/gene delivery and disease diagnostics. ¹⁴⁻¹⁸ As nucleic acids are negatively charged, the CDs used for gene delivery are mainly pristine and modified cationic CDs (CCDs) which contain abundant positively charged amine groups. Owing to these amine groups, CCDs can bind negatively charged nucleic acids to form CCDs-nucleic acid complexes and attach on the surface of the cell membrane to promote endocytosis-based cellular uptake process. ¹⁹

64

65

66

67

68

69

70

71

72

73

74

75

76

77

78

79

80

81

82

83

84

85

86

87

88

89

90

91

92

93

94

To prepare desirable CCDs for gene delivery, cationic substances such as polyethyleneimine (PEI), chitosan and poly-L-Lysine (PLL) have been used as precursors or grafted on the surface of CDs. 3, 19-21 Among them, PEI, a commercial gene delivery reagent, has been the most common used one for CCDs synthesis. For instance, Li et al. synthesized the orange emissive PEI-CDs using 1, 2, 4-triaminobenzene and PEI as precursors. It was found that these PEI-CDs could deliver siRNA targeting hepatoma-derived growth factor (HDGF) into glioblastoma cells and downregulate the expression of HDGF. ²⁰ Hashemzadeh et al. prepared the arginine conjugated PEI-CDs (CD-PEI_{1.8K}-Arg) for the delivery of pDNA. The results showed that the transfection efficiency of CD-PEI_{1.8K}-Arg was around 60% in human embryonic kidney (HEK 293) cells, higher than that of PEI_{25k} (around 40%), when the mass ratio of CD-PEI_{1.8K}-Arg to pDNA was 160:1. ²² Karimi's group reported the nitrogen- and zinc-dopped CDs which were synthesized by utilizing citric acid, branched PEI25k and zinc salts as precursors for the CRISPR plasmids and mRNA delivery. In optimized condition, the transfection efficiencies of prepared CDs to plasmids and mRNA were 2 times and 20 times greater than that of PEI_{25K}, respectively. ²³ To further broaden the application of CCDs in gene delivery, the development and modification of other types of CCDs without using PEI also become a new tendency regarding application of CDs in gene delivery. For instance, Hasanzadeh et al. have proved that PLL functionalized CDs showed no considerable toxicity and could deliver Cy5-tagged DNA to HEK 293 cells with the efficiency of 70 %. ²¹ Rezaei and Hashemi found chitosan-based CDs prepared via using chitosan, citric acid and arginine as precursors exhibited higher transfection efficiency than PEI. ³ The CDs from 3,5diaminobenzoic acid and citric acid could effectively deliver exogenous ROX-labelled DNA into nucleus of Hela cells with a transfection efficiency of 37.5%. ²⁴ Our previous work also demonstrated that the CDs prepared through citric acid and pentaethylenehexamine (PEHA) could successfully deliver pDNA into HEK 293 cells. ²⁵ These publications collectively contribute insights into the synthesis of novel CCDs and their potential applications in the field of gene

delivery. To further improve the transfection efficiency, strategic surface modification of CCDs will be a promising tool.

Lipids, the compounds containing hydrophilic head groups and hydrophobic tails, have a high affinity to cellular membranes and show abilities for cell membrane destabilization and endosome escape. According to published literature, lipids and their derivatives, especially which are incorporated with unsaturated fatty acid such as oleic acid (OA) as lipid tails, have been widely investigated for gene delivery as non-viral carriers to improve the transfection efficiency ²⁶⁻²⁹. Thus, in theory, conjugation of lipids with appropriate CCDs can be applied to make CCDs with good transfection efficiency. To test this hypothesis, the CCDs named as APCDs were firstly synthesized by a microwave-mediated approach using arginine (Arg) and PEHA as precursors, followed by conjugating with OA. Based on various mass ratios between APCDs and OA, the resulting APCDs-OA conjugates were categorized into APCDs-0.5OA, APCDs-1.0OA, and APCDs-1.5OA. Subsequently, the pDNA and siRNA binding capabilities of as-prepared materials were measured by agarose gel electrophoresis assay, UV-vis absorption and fluorescence emission spectroscopies. The cytotoxicity, cellular distribution and pDNA/siRNA transfection efficiencies of prepared APCDs-OA conjugates were investigated in HEK 293 and osteosarcoma (U2OS) cells. The intracellular trafficking of Cy3-siRNA and Cy3-DNA was performed to explore the delivery mechanism. Finally, the results showed that APCDs-OA conjugates all possess good pDNA transfection abilities, while APCDs-0.5OA especially display an excellent siRNA transfection efficacy. Our study provides a new perspective method on the designation of CCDs-based nonviral vehicles for gene delivery.

2. Experimental section

95

96

97

98

99

100

101

102

103

104

105

106

107

108

109

110

111

112

113

114

115

116

117

118

119

120

121

122

123

124

2.1 Materials and reagents

L-Arginine monohydrochloride (Arg, ≥ 98%), pentaethylenehexamine (PEHA), N-(3-dimethylaminopropyl)-N'-ethylcarbodiimide hydrochloride (EDC), N-hydroxysuccinimide (NHS, 97%), oleic acid (OA, 90%), branched polyethylenimine (PEI, 25kDa), calf thymus sonicated DNA and thiazolyl blue tetrazolium bromide (MTT) were bought from Sigma-Aldrich (St Louis, MO, USA). Green fluorescence protein (GFP) plasmids were purchased from VectorBuilder (Santa Clara, CA, USA). Western Blotting Substrate and NucRed Dead 647 were purchased from Thermo Fisher Scientific (Waltham, MA, USA). NMouse anti-GFP antibody (CAT# SC-9996) and anti-

mouse IgG secondary antibodies (CAT# 926-32210 and 102673-408) were bought from Santa Cruz (Dallas, TX, USA) and LI-COR (Lincoln, NE, USA), respectively. The rabbit polyclonal anti-FANCA (catlog# A301-980A; RRID: AB 1547945) antibody and anti-FANCD2 antibody (catlog# 28619-1-AP) were obtained from Bethyl Laboratories (Montgomery, TX, USA) and Proteintech (San Diego, California, USA), respectively. The Cy3 labeled-DNA (Cy3-DNA) were obtained by Polymerase Chain Reaction (PCR). The Cy3 labeled siRNA (Cy3-siRNA) (MISSION® siRNA Fluorescent Universal Negative Control #1, Cyanine 3) was purchased from Sigma-Aldrich (St Louis, MO, USA). FANCA siRNA (L-019283-00-05) and FANCD2 siRNA (L-016376-00-05) were ordered from Dharmacon (Lafayette, CO, USA). LumiTracker Lyso green was bought from Lumiprobe (MD, USA). Hoechst 33342 was obtained from Thermo Fisher Scientific (USA). The Biotech CE Dialysis Tubing with 100-500 Da molecular weight cut-off was obtained from Spectrum Laboratories (Rancho Dominguez, CA, USA). The deionized (DI) water was purified via a Modulab 2020 water purification system acquired from Continental Water System Corporation. (San Antonio, TX, USA). The purified DI water possesses a resistivity of 18.2 MΩ.cm and a surface tension of 72.6 mN·m⁻¹ at 22 °C. All the reagents were used without further purification.

2.2 Synthesis of APCDs

The APCDs were synthesized through the microwave method with Arg and PEHA as precursors. In detail, 500 mg of Arg and 500 µL of PEHA were dissolved in 25 mL of DI water. After vigorous stirring overnight, the solution was microwaved at 700 W for 7 min and naturally cooled down to room temperature. Subsequently, the product was dispersed in 20 mL of DI water and ultrasonicated for 5 min, followed by ultracentrifugation twice at 9000 rpm for 20 min. The supernatant solutions were collected, filtered using a 0.2 µm Sterile and Non-Pyrogenic Polyethersulfone Membrane, and dialyzed for 3 days in a 100-500 Da molecular weight cut-off dialysis tubing against DI water that was replaced every 24 h. Finally, the resulting solution was lyophilized for 3 days to obtain the APCDs powders.

2.3 Synthesis of APCDs-OA conjugates

The APCDs-OA conjugates were synthesized via a classic EDC/NHS-mediated amidation reaction. By varying the mass ratio of APCDs to OA from 1:0.5 to 1:1 and 1:1.5, three products, namely APCDs-0.5OA, APCDs-1.0OA and APCDs-1.5OA were prepared, respectively. Briefly, to

synthesize APCDs-0.5OA, 25 mg of OA was dissolved in 6 mL of ethanol. Then a solution 155 containing 137 mg of EDC in 0.5 mL of DI water was added and stirred for 30 min. Thereafter, 156 157 0.5 mL of NHS solution with 102 mg of NHS was added, stirred for 30 min, and mixed with 3 mL of APCDs solution that contained 50 mg of APCDs. The reaction mixture was further agitated for 158 24 h and purified using a 100-500 Da molecular weight cut-off dialysis tubing against DI water 159 for 3 days. The final product of APCDs-0.5OA was obtained after freeze drying for 3 days. APCDs-160 1.00A and APCDs-1.50A were prepared via the similar method as above by changing 25 mg of 161 OA to 50 and 75 mg of OA, respectively. 162

2.4 Characterization

163

164

165

166

167

168

169

170

171

172

173

174

175

176

177

178

179

180

181

182

183

184

AFM and TEM images were recorded by a 5420 atomic force microscope (Agilent Technologies, USA) and a 1200X transmission electron microscope (TEM) (JEOL, USA), respectively. For preparation of TEM samples, nanoparticles were dispersed in DI water with a concentration of 0.1 mg/mL. One dropwise of solution was added on Formvar Film 150 Mesh (Cu) and dried for TEM imaging. The absorption spectra were performed with a Cary 100 UV-vis spectrophotometer (Agilent Technologies, USA), while the fluorescence spectra were obtained on a Fluorolog-3 fluorometer (Horiba Jobin Yvon, USA) using 1 cm-pathlength cuvettes. FTIR spectra were collected from a PerkinElmer Fourier-transform infrared spectrometer (Frontier, PerkinElmer, USA) with Smart Orbit attenuated total reflectance accessories (Thermo Scientific, USA). XPS results were obtained from a PHI 5000 Versa Probe (Physical Electronics, Chanhassen, MN) scanning X-ray photoelectron spectrometer coupled with a monochromatic Al K-alpha X-ray source with 1486.6 eV of energy, 15 kV of voltage, and 1 mA of anode current. Zeta potential was measured by a Malvern Zetasizer (Malvern Panalytical, USA). Thermogravimetric analyses (TGA) and derivative thermogravimetry (DTG) were individually performed on a TG 209 F3 Tarsus thermo-microbalance (Netzsch, USA) while being heated from 40 to 1000 °C at a rate of 10 °C/min under a nitrogen gas flow.

2.5 Agarose gel electrophoresis

To investigate the pDNA and siRNA binding effect of APCDs and APCDs-OA conjugates, agarose gel electrophoresis experiments were conducted. For pDNA binding, APCDs or APCDs-OA conjugates (APCDs-0.5OA, APCDs-1.0OA and APCDs-1.5OA) were mixed with 200 ng of pDNA at different mass ratios of 0.5:1, 1:1, 2:1, 4:1 and 8:1, followed by incubation for 30 min at

37 °C to obtain APCDs-pDNA or APCDs-OA conjugate-pDNA complexes. Then, the complex samples were loaded on a 0.9% agarose gel, run for 70 min at 130 V in Tris-acetate-EDTA (TAE) buffer (pH 8.3), and stained by ethidium bromide (EB) dye for 15 min. Finally, the gel was imaged via a BioRad-image lab software to capture the migration bands of pDNA.

With respect to siRNA binding, APCDs or APCDs-OA conjugates were mixed with 100 ng of siRNA at varying mass ratios of 10:1, 20:1, 40:1, 80:1 and 160:1. After incubation for 30 min at 37 °C, the acquired samples were loaded on a 1% agarose gel containing EB and run for 60 min at 70 V in TAE buffer (pH 8.3) for further siRNA band imaging.

2.6 Cytotoxicity experiments

The cytotoxicity assessment of APCDs, APCDs-OA conjugates and PEI in U2OS and HEK 293 cell lines were conducted through the MTT assay. Briefly, U2OS cells were seeded in a 96-well plate at the density of 5×10^3 cells/well, while HEK 293 cells were seeded at a density of 4×10^3 cells/well. The cell culture medium in each well was 200 μ L of Dulbecco's modified Eagle medium (DMEM) supplemented with 10% of fetal bovine serum (FBS) and 1% of penicillin-streptomycin. The cells were then incubated for 24 h at 37 °C in a humidified atmosphere and 5% CO₂. After incubation, the medium was aspirated. The fresh DMEM containing various concentrations (0, 1.66, 3.13, 6.25, 12.5, 25, 50, and 100 μ g/mL) of APCDs, APCDs-0.5OA, APCDs-1.0OA, APCDs-1.5OA or PEI was added to the respective wells. The cells were further incubated for 48 h under the same conditions. Subsequently, 20 μ L of a 5 mg/mL 3-(4,5-dimethyl-2-thiazolyl)-2,5-diphenyl-2H-tetrazolium bromide (MTT) was added to each well, followed by a 4 hour-incubation. The culture medium was discarded and 150 μ L of dimethyl sulfoxide (DMSO) was added to dissolve the formazan crystals formed during the assay. The absorbance of each well was measured at 595 nm using a Tecan Microplate Reader.

2.7 Cellular distribution of APCDs and APCDs-OA conjugates

U2OS cells were seeded into an 8-well chamber slide which contained 300 μ L of DMEM in each well at a density of 2 \times 10⁴ cells/well. Following a 24-hour-incubation, the medium was substituted with fresh DMEM containing a concentration of 1.0 mg/mL of either APCDs, APCDs-0.5OA, APCDs-1.0OA or APCDs-1.5OA. The cells were then incubated for 1 h, fixed by 4% paraformaldehyde (PFA) for 15 min, and stained by NucRed Dead 647 dye for 1 h at room temperature. Finally, the cells were mounted for further cell imaging which was performed on a

Zeiss 880 confocal microscope. The HEK 293 cells were seeded in a 35 mm glass-bottom dish at a density of 6 × 10⁴ cells per well. After incubation of 24 h, the medium was replaced with fresh DMEM containing 1.0 mg/mL of APCDs, APCDs-0.5OA, APCDs-1.0OA or APCDs-1.5OA, followed by incubation for 4 h. The medium was 2 mL per dish. The cells were then fixed by PFA, stained by NucRed Dead 647 dye, and mounted for imaging.

2.8 Delivery of pDNA

The pDNA that expresses green fluorescence protein (GFP) was used to investigate the transfection efficiency of APCDs and APCDs-OA conjugates. Specifically, U2OS and HEK 293 cells were seeded in 35 mm glass-bottom dishes at a density of 2.5 × 10⁵ and 6 × 10⁴ cells/dish, respectively, in 2.0 mL of DMEM (10% of FBS and 1% of penicillin-streptomycin), followed by incubation for 24 h at 37°C. Then, the APCDs-pDNA or APCDs-OA conjugate-pDNA complexes were prepared by mixing APCDs, APCDs-0.5OA, APCDs-1.0OA, or APCDs-1.5OA with 1 μg of pDNA at different mass ratios (20:1 and 40:1) for a 30-minute incubation in 200 μL of DMEM. The PEI-pDNA complexes with a mass ratio of 2:1 was prepared by the same method as a positive control. The obtained complexes were added to cells. The expression of GFP in HEK 293 and U2OS cells were visualized through a Zeiss 880 confocal microscope and Zeiss fluorescence microscope, respectively. The transfection efficacy was quantitatively measured using Western Blot analysis. The cell viability of HEK 293 and U2OS cells after transfection with pDNA were detected by MTT assay.

2.9 Delivery of siRNA

U2OS cells were seeded at a density of 2.5×10^5 cells/well in a 6-well plate with 2 mL of DMEM and incubated for 24 h. Similar to the transfection process for pDNA, before delivering siRNA, 1 µg of either FANCA siRNA or FANCD2 siRNA was mixed with 40 µg of APCDs, APCDs-0.5OA, APCDs-1.0OA, or APCDs-1.5OA in 200 µL of DMEM. The mixture was incubated for 30 min to enable the formation of APCDs-siRNA or APCDs-OA conjugate-siRNA complexes. Subsequently, the complexes were added to cells. After incubating for 48 h, the cells were harvested for Western Blot analysis. The cell viability of U2OS cells after transfection with siRNA was measured by MTT assay.

For Western Blot analysis, in brief, the cells were detached using trypsin, washed with phosphate buffered saline (PBS) three times, and lysed on ice for 20 min using cell lysis buffer

containing a protease/phosphatase inhibitor cocktail. Following centrifugation at 12000 rpm for 15 min at 4 °C, the supernatant containing the cellular proteins was collected. The protein content of the extracted samples was determined by the BCA protein assay. 25 μg of total protein was loaded onto a gradient gel, separated by SDS–PAGE, and transferred to a PVDF membrane. The membrane was blocked with 5% milk in 0.1% Tween 20 in Tris-buffered saline (TBST) for 1 h. The membrane was then incubated overnight at 4 °C with anti-human FANCA antibody or antihuman FANCD2 antibody, along with anti-β-actin as loading control. After washing the membrane three times with TBST, a secondary antibody was applied and incubated for an additional hour. The resulting blots were visualized using Thermo Scientific Pierce ECL Western Blotting Substrate, enabling the detection of protein bands.

2.10 Intracellular trafficking

U2OS cells were seeded in a 35 mm glass-bottom dish at a density of 2.5×10^5 cells/dish and incubated for 24 h. The medium was 2 mL of DMEM. Then, the APCDs-0.5OA-DNA or APCDs-0.5OA-siRNA complexes were prepared by mixing 40 μ g of APCDs-0.5OA with 1 μ g of Cy3-DNA or Cy3-siRNA in 200 μ L of DMEM with incubation for 30 min. The complexes were added to cells. After incubation for 1, 2 and 4 h, the cells were washed with PBS and stained with Hoechst 33342 (2 μ g/mL) for 15 min and LumiTracker Lyso green (75 nM) for 10 min. Finally, the cells were imaged by Zeiss 880 confocal microscope.

2.11 Statistical analysis

All the experiments were performed at least triplicates. The data of cell viability and Western blot analysis are expressed as mean \pm standard error of the mean (SEM). Statistical significance between treated groups and control is determined by using the one-way analysis of variance (ANOVA) in GraphPad Prism 10.

3. Results and discussion

3.1 Characterization

273

274

275

276

277

278

279

280

281

282

283

284

285

286

287

288

289

290

291

292

293

In this research, the APCDs were synthesized by a microwave method and modified with OA for gene delivery application. The morphologic characterizations from AFM and TEM (Figure 1A) and Figure 1B) show that APCDs are uniformly dispersed nanoparticles with an average size of 1.2 nm in z-axis and 2.0 nm along the xy-plane (**Figure 1C**). They possess an excitation-dependent photoluminescence behavior with a maximum emission wavelength of 425 nm when excited at 350 nm (Figure 1D). Regarding the optical absorption properties, as-prepared APCDs exhibit two major absorption peaks at 233 and 290 nm in the UV-vis spectrum (Figure S1A), which are corresponding to π - π * transitions of C=O bonds and n- π * transitions of C=N/C=O bonds, respectively. OA (Figure 1E) has one characteristic peak at 228 nm that can be ascribed to n- π * transitions of C=O bonds from the carboxylic group. Upon conjugating APCDs with OA at various mass ratios, the acquired APCDs-0.5OA, APCDs-1.0OA and APCDs-1.5OA all exhibit a new absorption peak at 257 nm, while the peaks related to APCDs at 233 and 290 nm disappeared. The new peak at 257 nm can be assigned to the n- π * transitions of amide bonds formed by carboxylic groups of OA and amine groups of APCDs, suggesting the successful conjugation. With the increase amount of OA, the absorbance at 257 nm is increased as well. Figure S1B to 1D display the emission spectra of APCDs-OA conjugates. As can be seen, even though the concentration of APCDs-OA conjugates are 5 times higher than that of APCDs, the fluorescence intensities of APCDs-0.5OA, APCDs-1.0OA and APCDs-1.5OA are still lower than that of APCDs. It further suggests the successful conjugation of OA with APCDs.

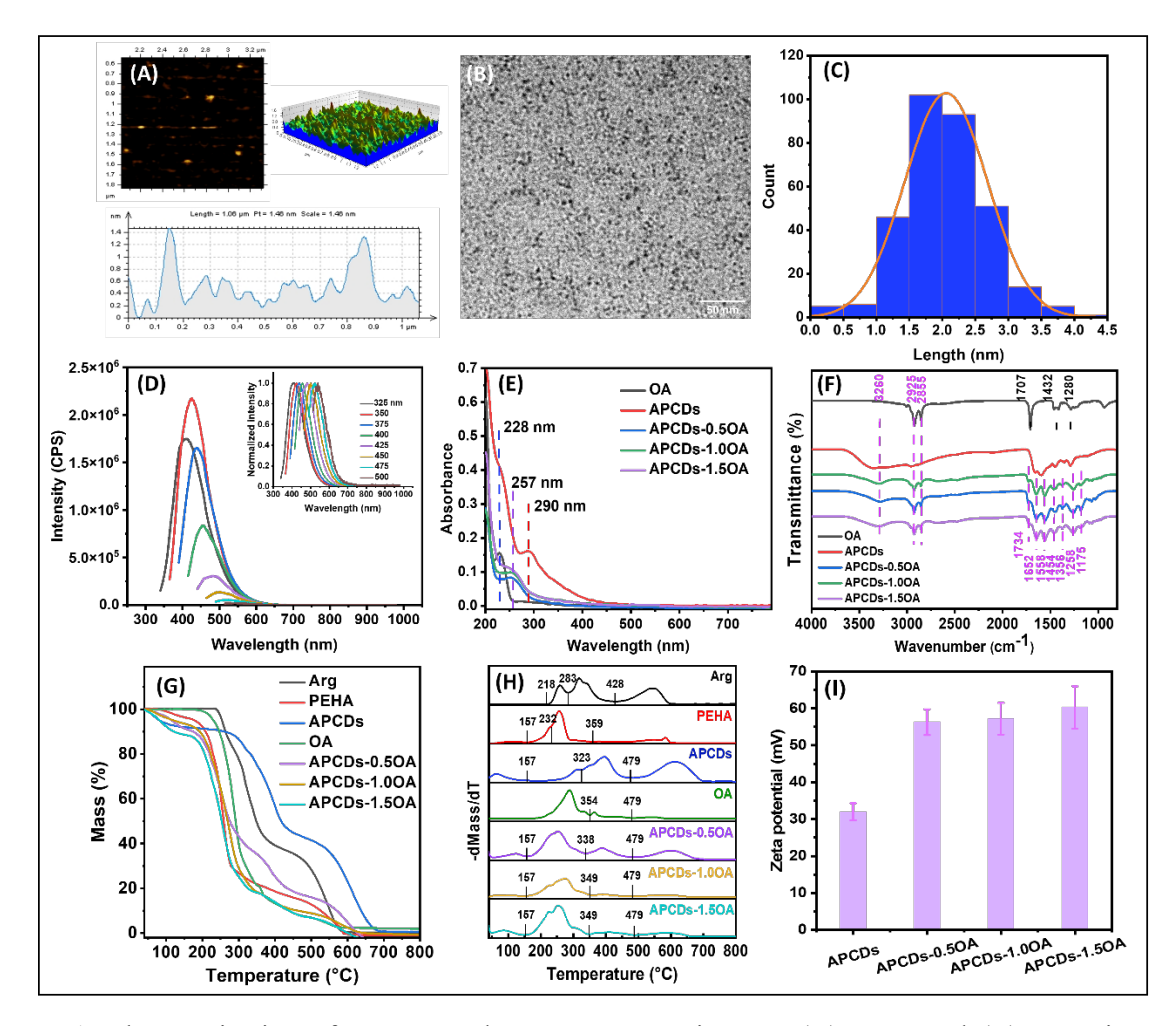


Figure 1. Characterization of APCDs and APCDs-OA conjugates: (A) AFM and (B) TEM images of APCDs. (C) Size distribution histogram and (D) fluorescence emission spectra of APCDs at 1 μg/mL. (E) UV-vis and (F) FTIR spectra of OA, APCDs, APCDs-0.5OA, APCDs-1.0OA, and APCDs-1.5OA; the insets are the normalized fluorescence spectra. (G) TGA and (H) DTG of Arg, PEHA, APCDs, OA, APCDs-0.5OA, APCDs-1.0OA and APCDs-1.5OA. (I) Zeta potential of APCDs, APCDs-0.5OA, APCDs-1.0OA and APCDs-1.5OA.

To identify the functional groups in the prepared materials, FTIR analysis was conducted on the precursors (Arg and PEHA), APCDs and APCDs-OA conjugates. The FTIR spectra are presented in **Figure S2**, **Figure 1F** and summarized in **Table S1**. From the spectra of precursors (**Figure S2**), both Arg and PEHA exhibit the characteristic bands corresponding to N-H stretching vibrations of amine groups. Specifically, the bands were found at 3353 and 3151 cm⁻¹ for Arg and 3279 cm⁻¹ for PEHA. Moreover, the bending vibrations of N-H bonds in Arg and PEHA were observed at 1566 and 1593 cm⁻¹, respectively. These results indicate the presence of amine groups in both Arg and PEHA, suggesting their potential for synthesizing CDs with positive charges. Along with the band of C-H bending vibrations at 1454 cm⁻¹, the appearance of C-H stretching

vibrational peaks at 2868 cm⁻¹ for Arg as well as 2932 and 2811 cm⁻¹ for PEHA confirm the alkyl structures within precursors. ^{25, 30, 31} In addition to the common moieties mentioned above, Arg also shows the typical C=O stretching vibrational band at 1679 cm⁻¹ and C=N stretching vibrational band at 1638 cm⁻¹. Meanwhile, three bands related to C-N, C-C, and C-O stretching vibrations were found at 1404, 1318 and 1180 cm⁻¹, respectively. ³⁰ For Arg, the C-N and C-C stretching bands were observed at 1356, 1291 and 1118 cm⁻¹. Using FTIR spectra of Arg and PEHA as references, in Figure S2, the broad band of APCDs at 3374 cm⁻¹ is attributed to N-H stretching vibrations, which confirms the existence of amine groups. The peaks at 2951, 1660, 1593 and 1454 cm⁻¹ are assigned to C-H stretching, C=O/C=N stretching, N-H bending and C-H bending vibrations, respectively. The stretching vibrational bands of C-N and C-C were identified at 1356 and 1291 cm⁻¹, respectively. Regarding APCDs-OA conjugates, all the spectra of APCDs-0.5OA, APCDs-1.0OA and APCDs-1.5OA in Figure 1F reveal three of new peaks at 2925, 2855 and 1734 cm⁻¹ when compared to FTIR spectrum of APCDs. Among these peaks, the ones at 2925 and 2855 cm⁻¹ completely overlap with the C-H stretching vibrational bands of OA, indicating the potential presence of octadecene originating from OA in structures. The one at 1734 cm⁻¹ corresponds to the C=O stretching vibrations of amide bonds formed by amine groups of APCDs and carboxyl groups of OA, which is distinct from the C=O stretching vibrations of carboxy groups at 1707 cm⁻¹ in pure OA. 32 Meanwhile, after conjugating, the N-H stretching vibrations and N-H bending vibrations of APCDs were shifted from 3374 to 3260 cm⁻¹ and 1593 to 1558 cm⁻¹, respectively. All these differences between APCDs-OA conjugates and APCDs demonstrate the successful conjugation of OA with APCDs via amidation reaction.

310

311

312

313

314

315

316

317

318

319

320

321

322

323

324

325

326

327

328

329

330

331

332

333

334

335

336

337

338

339

340

To confirm the surface structures of as-synthesized materials, the elemental compositions of APCDs and APCD-OA conjugates were characterized by XPS. As listed in **Table S2**, APCDs and APCDs-OA conjugates all have three major elements including carbon, oxygen, and nitrogen on their surface. Compared to the APCDs, APCDs-OA conjugates exhibit an increasing amount of carbon and oxygen with a decrease amount of nitrogen. Upon the increase of OA in the conjugation process, the percentage of carbon has increased from 76.2% in APCDs to 83.1%, 85.6% and 87.2% in APCDs-0.5OA, APCDs-1.0OA and APCDs-1.5OA, respectively, which might infer the successful conjugation between APCD and OA. The high-resolution XPS spectra and functionalities analysis of C 1s, O 1s and N 1s of as-prepared APCDs and APCDs-OA conjugates are displayed in **Figure S3** and **Table S3**. As shown in **Figure S3**, all the C1s spectra of APCDs

and APCDs-OA conjugates can be deconvoluted into three peaks at around 284.3, 285.8 and 287.9 eV, which can be attributed to sp³ hybridized carbon, C-N and carboxylic/imine groups, respectively. Among them, the contents of sp3 hybridized carbon (Table S3) of APCDs-0.5OA (57.1%), APCDs-1.0OA (78.8%) and APCDs-1.5OA (70.4%) are significantly higher than that of APCDs (44.7%), suggesting the presence of octadecenoic carbonic long chains from OA on the surface of APCDs-OA conjugates. The marginal change of percentage of sp3 carbon between APCDs-1.0OA and APCDs-1.5OA demonstrates the saturation of OA. Additionally, the O 1s spectra fitted with two peaks at 532.8 and 530.3 eV are attributed to carboxylic and amide bonds, respectively. For N 1s spectra, three peaks that can be assigned to imine (398.1 eV), amine (399.3 eV), and amide residues (400.4 eV) were observed. ^{2,24,33-35}

Both TGA (Figure 1G) and DTG (Figure 1H) were performed on Arg, PEHA, APCDs, OA, APCDs-0.5OA, APCDs-1.0OA and APCDs-1.5OA to learn their thermal stabilities and structural compositions. In comparison, APCDs have a higher thermal stability than Arg and PEHA, which is suggested by the temperature increase for a complete decomposition. It was observed that OA conjugation didn't significantly affect the thermal stabilities of APCDs. Distinct DTG of Arg, PEHA, and APCDs indicate the formation of APCDs, while similar DTG of APCDs-0.5OA, APCDs-1.0OA and APCDs-1.5OA exhibit the decomposition of both APCDs and OA, demonstrating the successful conjugation between APCDs and OA. Structural composition information of different materials was obtained by referring to our previous studies. ^{36, 37} In the studies, mass loss at 40-168, 168-338, 338-448, and 448-1000 °C represents evaporation of water molecules, decomposition of oxygen-containing functional moieties and/or sublimation of small carbon frameworks, amines, and graphene-like or carbon nitride structures, respectively. However, considering the boiling points of Arg (368 °C), PEHA (136-144 °C) and OA (360 °C), their decompositions might not entirely follow these rules. For instance, for Arg, the decomposition at 218-283 °C can be ascribed to the loss of -COOH. The actual mass loss was 17%, which is comparable to the theoretical value of 26%. However, due to the boiling point of Arg at 368 °C, the subsequent mass losses were due to a combination of decomposition and volatilization. Regarding OA, since it is composed of -COOH and small carbon frameworks, before volatilization at 360 °C, about 80% mass loss occurred due to decomposition.

Different from small molecules, APCDs and APCDs-OA conjugates display complex decomposition processes. The decomposition stages with corresponding decomposed structures

were speculated and shown in **Table S4**. As it can be seen, bare APCDs possess 8% of adsorbed water molecules or hydroxyl groups, 10% of oxygen-containing functional moieties and/or small carbon frameworks, and 39% of amines, which accounts for the shell percentage of APCDs (57%). After conjugation to OA, the content of oxygen-containing functional moieties and/or small carbon frameworks was increased to 54%, 74%, and 70% for APCDs-0.5OA, APCDs-1.0OA, and APCDs-1.5OA, respectively, while the content of amines was decreased. Similar contents of oxygen-containing functional moieties and/or small carbon frameworks between APCDs-1.0OA and APCDs-1.5OA might indicate saturation of OA on the surface of APCDs. Additionally, the percentage of shell significantly increased after conjugation, providing further confirmation of the successful conjugation between APCDs and OA.

372

373

374

375

376

377

378

379

380

381

382

383

384

385

386

387

388

389

390

391

392

393

394

395

396

397

398

399

400

401

Confirming the successful synthesis of APCDs and APCDs-OA conjugates, a zeta potential analysis was conducted to investigate whether these materials exhibit positive charges. As depicted in Figure 1I, the zeta potential of APCDs is appropriate 32 ± 2.3 mV, while that of APCDs-0.5OA, APCDs-1.0OA and APCDs-1.5OA is 56.3 ± 3.5 , 57.2 ± 4.3 and 60.3 ± 5.7 mV, respectively. Compared to APCDs, all the APCDs-OA conjugates exhibit significantly increased zeta potential. According to theories in published literatures, this phenomenon might be attributed to the amphiphilic properties of APCDs-OA conjugates in structure. ^{7, 38-40} Amphiphilic APCDs-OA conjugates composed of hydrophilic APCDs, and hydrophobic OA tails may self-assemble or aggregate because of the decrease of water solubility. In this system, hydrophobic interactions between APCDs-OA conjugates, dominated by OA, and hydrophilic properties of APCDs may promote the formation of a core-shell structure, in which some OA tails may form a network in the core, while the positively charged APCDs are distributed in the shell. Consequently, APCDs-OA conjugates might form a partial micelle-like structure, increasing the zeta potential due to the exposure of a large number of APCDs in self-assemble system. To test such hypothesis and investigate the size difference between APCDs and APCDs-OA conjugates, APCDs, APCDs-0.5OA, APCDs-1.0OA or APCDs-1.5OA at a concentration of 0.1 mg/mL was dispersed in water and then dried on a Formvar Film for TEM imaging. As shown in Figure S4, APCDs-OA conjugates exhibit aggregation or self-assembly. The sizes of these self-assemblies or aggregations for APCDs-0.5OA, APCDs-1.0OA, and APCDs-1.5OA are 18.3 ± 3.8 , 33.9 ± 5.7 , and 33.8 ± 8.8 nm, respectively. With an increase in OA content, the sizes of self-assemblies or aggregations

increase, demonstrating that hydrophobic interactions which are mainly derived from OA play a vital role in the self-assembly or aggregation process.

3.2 DNA and siRNA binding experiments

3.2.1 Agarose gel electrophoresis and complex evaluation

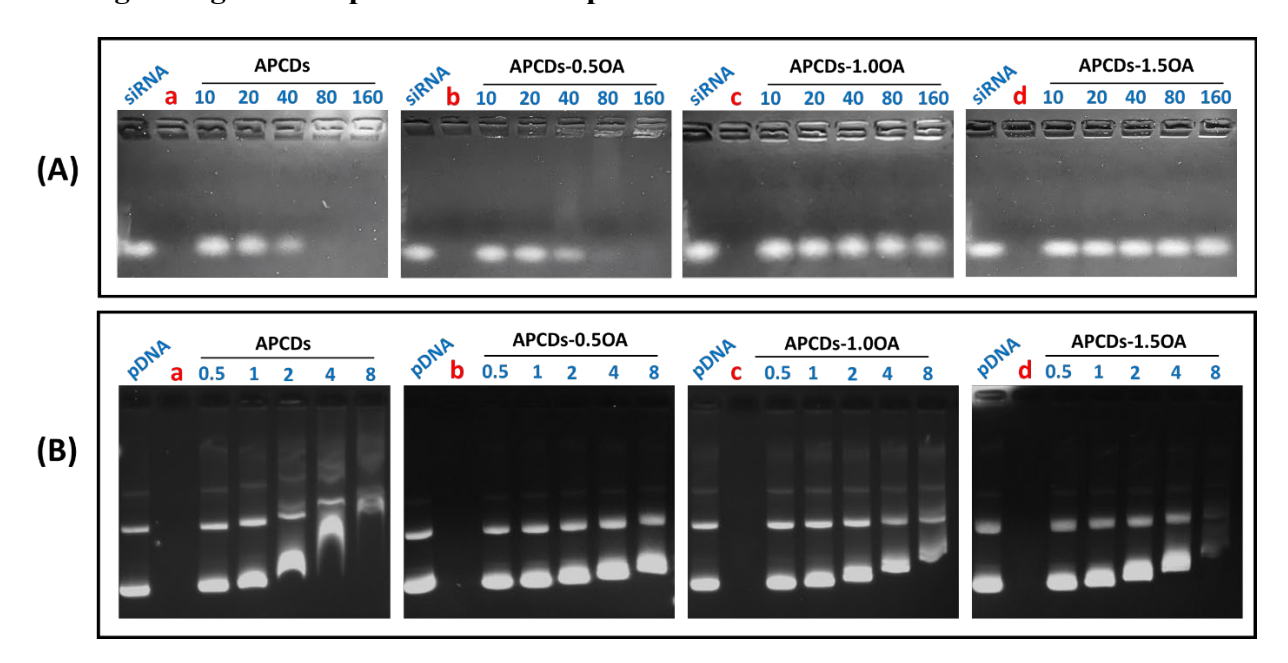


Figure 2. The agarose gel electrophoresis analysis of materials APCDs, APCDs-0.5OA, APCDs-1.0OA and APCDs-1.5OA bound with (A) siRNA and (B) pDNA at different mass ratios of the material to siRNA or pDNA; a, b, c, and d represent the samples only contain APCDs, APCDs-0.5OA, APCDs-1.0OA and APCDs-1.5OA, respectively.

The nucleic acid binding abilities of vehicles play a crucial role in gene delivery applications. In theory, the negatively charged nucleic acids with a phosphate backbone structure would interact with positively charged materials through electrostatic interactions. ^{22,23} Since we have proved that the as-prepared materials, including APCDs and APCDs-OA conjugates, all carry positive charges, agarose gel electrophoresis experiments were performed to investigate their affinity to siRNA and pDNA. As displayed in **Figure 2**, both naked siRNA and pDNA show standard migration bands. In contrast, no bands were observed for the naked APCDs and APCDs-OA conjugates. When APCDs or APCDs-OA conjugates were mixed with siRNA, both the migration and intensity of the siRNA bands were reduced depending on concentrations of APCDs or APCDs-OA (**Figure 2A**). Especially, for APCDs and APCDs-0.5OA, as the mass ratio increased to 80:1 or higher, migration of the siRNA was completely retarded, conforming an effective siRNA binding. However, for APCDs-1.0OA and APCDs-1.5OA, only a slight reduction in band migration was observed, even

when the mass ratio was increased to 160:1, indicating a weak siRNA binding. These data suggest that appropriate amount of OA does not affect APCDs and siRNA interaction, but extra amount of OA results in deceased binding ability to siRNA. It might be because the excess OA that is not in core of APCDs-OA partial-micelles reduces the binding opportunities between siRNA and positively charged APCDs in APCDs-OA conjugates due to the steric effect.

Regarding pDNA binding (**Figure 2B**), upon increasing the mass ratio from 0.5:1 to 8:1, migration bands of the pDNA mixed with APCDs or APCDs-OA conjugates all become slower. Similar to siRNA binding, the conjugation of OA with APCDs to form APCDs-OA conjugates reduces the pDNA binding capability compared to APCDs alone. Thus, the agarose gel electrophoresis results demonstrate that all APCDs and APCDs-OA conjugates can successfully bind with pDNA, while APCDs and APCDs-0.5OA exhibit much better siRNA binding capability than that of APCDs-1.0OA and APCDs-1.5OA. As the pDNA used for the binding is around 5000 bp (base pair) and the siRNA is around 21 bp, the significant difference between pDNA and siRNA binding might be highly related to the size of pDNA and siRNA. Detailly, pDNA with tremendous more bp and larger size can provide more binding sites to carriers than that of siRNA. In this situation, even though the presence of OA might affect the binding between pDNA and APCDs-OA conjugates because of the steric effect, the enormous number of binding sites still could enable the APCDs-OA conjugate-pDNA complex formation, especially for APCDs-1.0OA and APCDs-1.5OA. Furthermore, these binding sites make APCDs-OA conjugate-loaded pDNA show apparently slower migration of band even when the mass ratios are equal or below 8:1.

The zeta potential of APCDs and APCDs-OA conjugates with the addition of different amounts of pDNA were measured to further investigate the appropriate mass ratio for pDNA binding. The results are displayed in **Figure S5**. As it can be seen, the zeta potential of both APCDs and APCDs-OA conjugates decreased with the addition of pDNA. When the mass ratios of APCDs to pDNA were lower than 5:1, the zeta potential reduced to zero. For APCDs-OA conjugates, negative charges were found when the mass ratios were less than 10:1, while the positive charges were still observed with the mass ratios equal or higher than 20:1. These results suggest that the complete binding between APCDs-OA conjugates and pDNA might only be achieved when the mass ratio is equal or higher than 20:1. The mass ratio of 40:1 lead to a positive charge in the range of 12.7 - 22.5 eV, which is beneficial for dispersion of formed complexes in aqueous system. Based on the results above, the sizes of APCDs-pDNA and APCDs-OA conjugate-pDNA complexes

formed by mass ratio of 40:1, were evaluated by TEM. As shown in **Figure S6A**, APCDs-pDNA complexes are irregular shape. In comparison, APCDs-OA conjugate-pDNA complexes are mostly well distributed with a spherical shape, which infers the presence of micelles structure-based complexes. The sizes of APCDs-0.5OA-pDNA, APCDs-1.0OA-pDNA and APCDs-1.5OA-pDNA (**Figure S6B-6D**) are 95.2 \pm 6.1, 118.9 \pm 16.3 and 111.42 \pm 19.8 nm, respectively. For siRNA binding, using APCDs-0.5OA as an example, similar spherical shape of APCDs-0.5OA-siRNA complexes (**Figure S6E**) were observed with the size of 102.2 \pm 14.7 nm. The release of pDNA from APCDs-pDNA or APCDs-OA conjugate-pDNA complexes investigated by agarose gel electrophoresis method are shown in **Figure S7**. With addition of heparin, the retarded pDNA were gradually released from complexes. When the mass ratio of heparin to pDNA was 50:1, they were almost released. Meanwhile, the release of pDNA from APCDs-pDNA complexes (**Figure S7A**) is easier compared to that from APCDs-OA conjugates-based complexes (**Figure S7B-7D**). This result indicates that the pDNA complexes formed by APCDs-OA conjugates might be more stable than those formed by APCDs.

3.2.2 UV-vis and fluorescence spectra

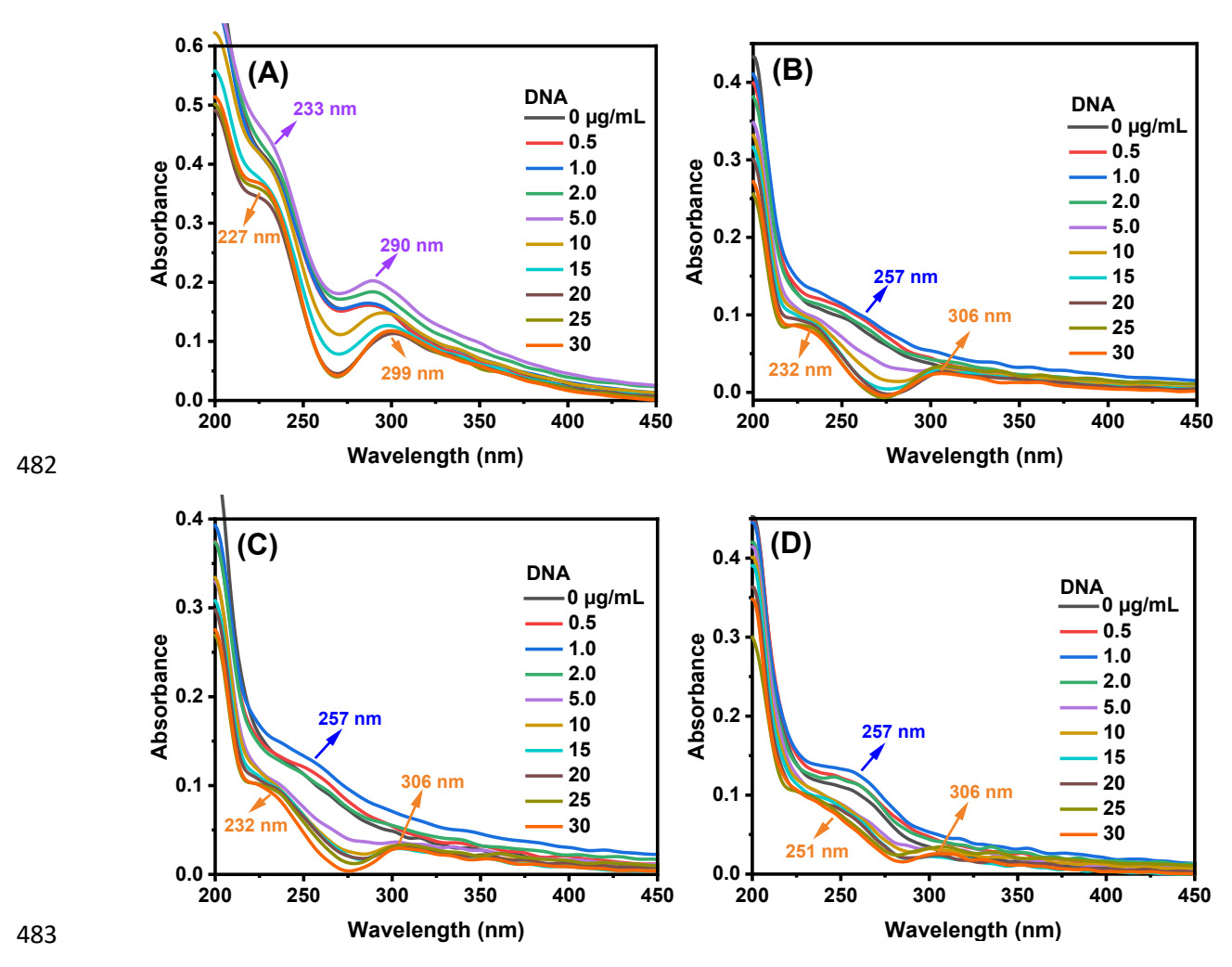


Figure 3. UV-vis absorption spectra of (A) APCDs, (B) APCDs-0.5OA, (C) APCDs-1.0OA and (D) APCDs-1.5OA at 20 μg/mL in the presence of different concentration of DNA.

To further investigate the binding affinity and binding mechanism of the synthesized materials to DNA, UV-vis absorption, and fluorescence emission spectra of APCDs and APCDs-OA conjugates with addition of calf thymus DNA were measured. In general, binding mechanisms of small molecules to DNA can be classified as covalent and non-covalent binding. The non-covalent binding can be further categorized into intercalative, groove and electrostatic interactions. In the UV-vis absorption spectra, any changes associated to the absorbance and wavelength of characteristic peaks of the molecules or DNA can serve as evidence for binding modes and binding strength analysis. Briefly, the covalent binding manifests as a hyperchromic and bathochromic effect in absorption maxima, while the non-covalent binding results in diverse changes corresponding to different interaction modes. Published literature suggests that hypochromic effect

accompanied by a noticeable red shift indicates intercalative interactions, while lower hypochromic or hyperchromic effect without a red shift signifies electrostatic interactions. Groove binding typically induces negligible or minor changes in the UV-vis absorption spectra. ⁴¹⁻⁴⁸ For fluorescence spectra, a significantly increased fluorescence emission is an indication of intercalative interactions. In the case of electrostatic and groove binding, it is possible to observe a reduced fluorescence intensity of molecules in the presence of DNA. ^{18,49}

496

497

498

499

500

501

502

503

504

505

506

507

508

509

510

511

512

513

514

515

516

517

518

519

520

521

522

The UV-vis spectra of APCDs and APCDs-OA conjugates in the presence of different concentrations of DNA are presented in Figure 3. To eliminate the absorbance of DNA itself, an aqueous solution that only contains DNA was used as a blank sample during detection. Regarding APCDs, as displayed in Figure 3A, an increase in DNA concentration from 0.5 to 30 μg/mL led to an initial rise in the absorption intensity of peaks at 233 and 290 nm, followed by a subsequently decrease. The concentration of 5 µg/mL can be considered as a threshold for this change, where the hyperchromism of the band at 290 nm reaches to 27.20 %, without any red or blue shift, suggesting the presence of electrostatic interactions between APCDs and DNA. When the concentration increased from 5 to 30 µg/mL, the peak at 233 and 290 nm shifts to 227 and 299 nm, respectively. The hypochromism of the peak at 290 nm is around 28.16 %, indicating an intercalative binding mode. Thus, the UV-vis spectra suggests that both electrostatic and intercalative interactions participate in APCDs and DNA binding. After connecting with OA, the obtained APCDs-OA conjugates exhibit a different tendency in absorption spectra related to DNA binding. As it can be seen from Figure 3B-3D, with addition of DNA, the absorbance of the characteristic band of APCDs-OA conjugates at 257 nm increased initially and then decreased, which is similar to that of APCDs. However, instead of a red shift, only a blue shift was observed in this band, suggesting that the binding between APCDs-OA conjugates and DNA might predominate by electrostatic interactions. Furthermore, when the concentration of DNA is higher than 10 µg/mL, a new absorption peak appears at 306 nm, which might represent a stable APCDs-OA conjugate-DNA complex formation. ⁵⁰ Such stable complexes are extremely important in gene delivery application.

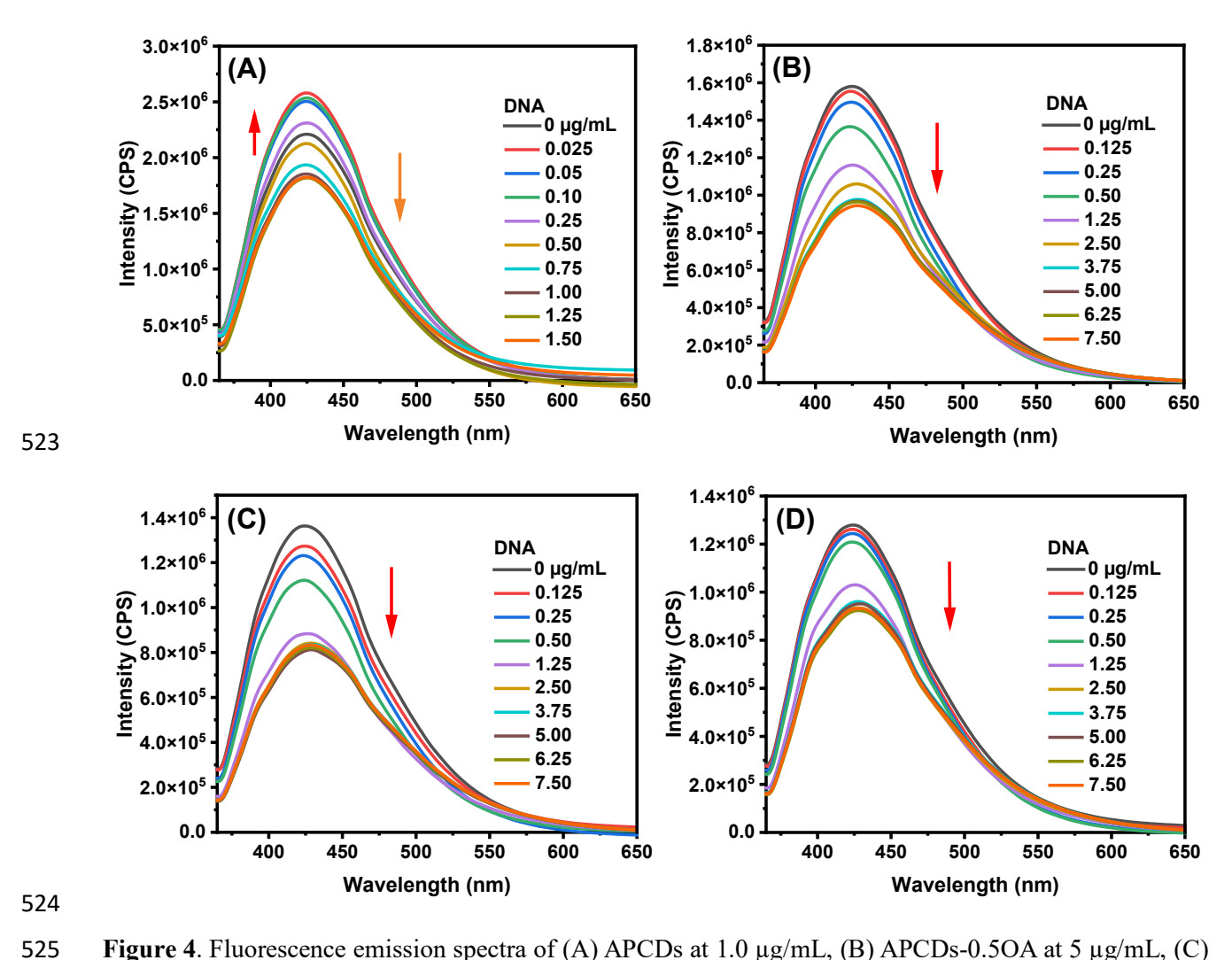


Figure 4. Fluorescence emission spectra of (A) APCDs at 1.0 μg/mL, (B) APCDs-0.5OA at 5 μg/mL, (C) APCDs-1.0OA at 5 μg/mL and (D) APCDs-1.5OA at 5 μg/mL in the presence of different concentrations of DNA.

The fluorescence spectra of APCDs and APCDs-OA conjugates with the addition of DNA are presented in **Figure 4**. As observed, the presence of DNA significantly affects the fluorescence intensity of APCDs and APCDs-OA conjugates. Specifically, from **Figure 4A**, the addition of DNA at a concentration lower than 0.25 μg/mL in APCDs solution enhances fluorescence intensity, while a deceased fluorescence intensity was observed when the concentration of DNA equals or higher than 0.5 μg/mL. Since **Figure 4A** illustrates both enhanced and quenched fluorescence, the interaction mechanisms between APCDs and DNA can be attributed to intercalative and electrostatic modes. At the highest DNA concentration of 1.50 μg/mL, the fluorescence quenching is approximately 18.2 %. Different from APCDs, APCDs-OA conjugates in **Figure 4B-4D** only show reduced fluorescence intensity, suggesting electrostatic interactions. With the addition of

DNA at 7.5 μg/mL, the fluorescence quenching for APCDs-0.5OA, APCDs-1.0OA and APCDs-1.5OA is 40.5%, 39.1% and 30.6%, respectively. As the change of the fluorescence intensity is strongly correlated with binding strength and complexes formation, the higher fluorescence quenching observed in APCDs-OA conjugates compared to APCDs suggests that APCDs-OA may form more stable complexes with DNA than APCDs. This might be because the APCDs-OA conjugates can bind with phosphate groups of DNA via external electrostatic interactions and then wrap the DNA in hydrophobic chain of APCDs-OA conjugates, forming the stable complexes like micelle-based complexes, which are consistent to the results shown in **Figure S6** and **Figure S7**.

3.3 Cytotoxicity assessment

MTT assays were conducted to investigate the cytotoxicity of APCDs and APCDs-OA conjugates in HEK 293 and U2OS cells. Meanwhile, the cytotoxicity of PEI was evaluated for comparison. As shown in **Figure 5A** and **5C**, PEI exhibits high cytotoxicity. When the concentration is 1.66 μ g/mL, the cell viability of HEK 293 and U2OS cells is 60% and 38%, respectively. In contrast, the as-prepared APCDs and APCDs-OA conjugates display significantly lower toxicity than PEI. At concentrations equal to or lower than 25 μ g/mL for APCDs and APCDs-OA conjugates, cell viabilities for both cell types exceed 70%. Furthermore, compared to pure APCDs, the conjugation of OA does not show a significant difference in cell viability. Based on the fitted curves in **Figure 5B** and **5D**, the half-maximal inhibitory concentration (IC50) values for APCDs, APCDs-0.5OA, APCDs-1.0OA, and APCDs-1.5OA in HEK 293 cells are 57.57, 56.85, 50.99, and 65.55 μ g/mL, respectively. In U2OS cells, the corresponding values are 57.57, 44.98, 48.63 and 47.99 μ g/mL, respectively. Hence, for further DNA and siRNA delivery studies, the concentration of APCDs and APCDs-OA conjugates would be maintained below 25 μ g/mL to minimize vehicle toxicity.

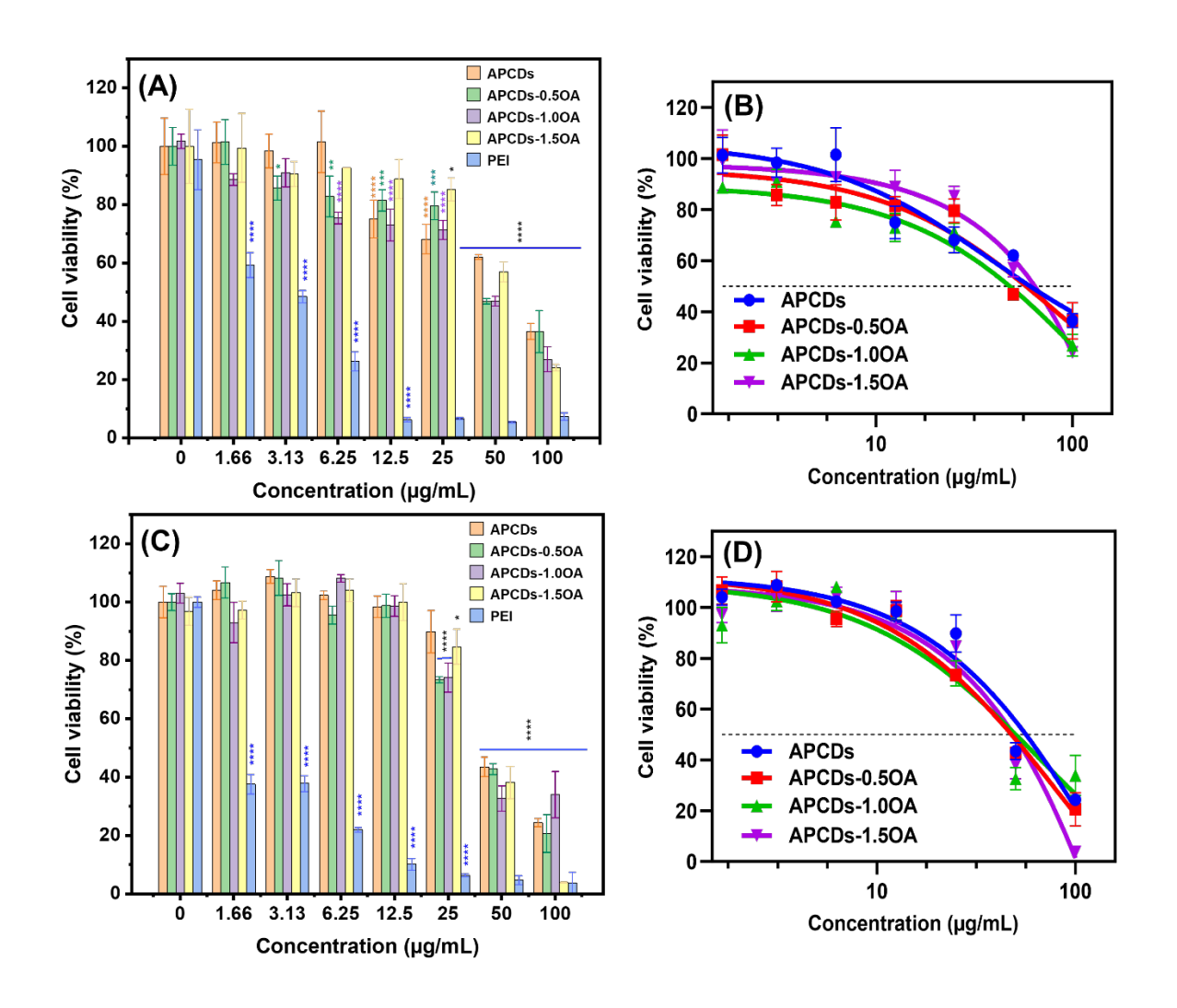


Figure 5. Cytotoxicity evaluation of APCDs, APCDs-0.5OA, APCDs-1.0OA and APCDs-1.5OA in (A) and (B) HEK 293, as well as (C) and (D) U2OS cells at the different concentration for 48 h at 37 °C. Data are shown as mean \pm SEM. Statistical significance is determined by using the one-way ANOVA analysis. *p<0.05, **p<0.01, ***p<0.001, ****p<0.001 compared to non-treated controls.

3.4 Cellular distribution of APCDs and APCDs-OA conjugates

It is well established that nucleic acids are negatively charged and face challenges in penetrating the cell membrane. Therefore, it is essential for a gene delivery carrier to have the ability to penetrate cell membranes and deliver exogenous DNA or RNA to their respective active sites. Since the active sites of normally used pDNA and siRNA are in cell nucleus and cytoplasm, respectively, ^{5, 51, 52} the evaluation of the intracellular distribution especially the nucleus targeting ability of APCDs and APCDs-OA conjugates is of great importance. The fluorescence microscopic images of HEK 293 and U2OS cells treated with APCDs and APCDs-OA conjugates are displayed in **Figure 6A** and **6B**, respectively. NucRed Dead 647 dye was applied to label the cell nucleus.

The results indicate that all APCDs and APCDs-OA conjugates can enter the cells and distribute in both the cytoplasm and nucleus. In addition, the cells incubated with APCDs-OA conjugates exhibit enhanced blue fluorescence in the nucleus compared with that of APCDs, demonstrating that the conjugation of OA on the surface of APCDs can improve the nucleus membrane penetration ability of the materials. This phenomenon is obviously observed in HEK 293 cells (**Figure 6A**). Therefore, the synthesized materials in this study may have potential to deliver pDNA and siRNA into their respective active sites within cells.

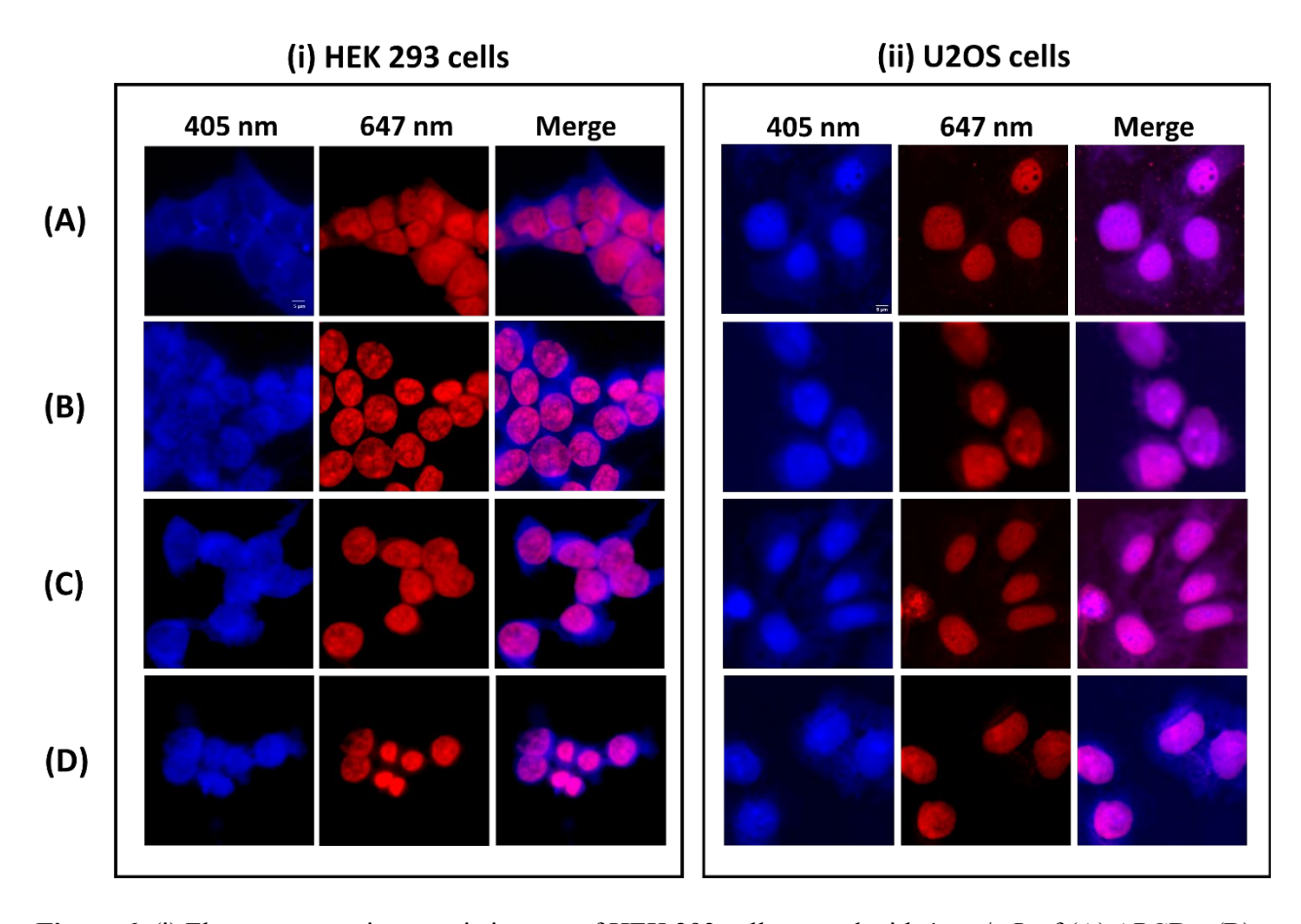


Figure 6. (i) Fluorescence microscopic images of HEK 293 cells treated with 1 mg/mL of (A) APCDs, (B) APCDs-0.5OA, (C) APCDs-1.0OA and (D) APCDs-1.5OA for 4 h; (ii) Confocal microscopic images of U2OS cells treated with 1 mg/mL of (A) APCDs, (B) APCDs-0.5OA, (C) APCDs-1.0OA and (D) APCDs-1.5OA for 1 h. NucRed Dead 647 dye was applied to label the cell nucleus.

3.5 Delivery of pDNA

590

591

592

593

594

595

596

597

598

599

600

601

602

603

604

605

606

607

608

609

610

611

The pDNA transfection efficiencies of as-prepared materials were assessed in HEK 293 and U2OS cells by delivering GFP plasmids. The mass ratio of the material to pDNA were set as 20:1 and 40:1. Cells treated only with pDNA were served as the negative control, while cells treated with PEI and pDNA were considered as the positive control. As can be seen in Figure S8, no green fluorescence protein signal was observed in cells treated only with naked pDNA, which indicates that pDNA alone cannot enter the cells and achieve gene expression. On the contrary, for the positive control, green fluorescence was observed in both types of cell lines. Among the assynthesized materials, APCDs fail to show transfection ability (Figure 7A and 7B). Despite confirming the pDNA binding capability of APCDs in agarose gel electrophoresis studies, the failure of GFP expression in cells might be because APCDs cannot protect pDNA from endosomal enzyme digestion in the intracellular environment. However, in comparison, after conjugating with OA, all the obtained APCDs-OA conjugates exhibit higher transfection efficiency than PEI. To understand whether the transfection ability was solely due to OA, the cells co-treated with OA and pDNA were also imaged, with the results shown in Figure S8. Since there were no signals observed under the green fluorescence channel, the high pDNA transfection efficiencies of APCDs-OA conjugates are attributed to the synergistic effect of APCDs and OA. Specifically, APCDs-OA conjugates with amphiphilic structure may encapsulate pDNA inside the structure to form stable complexes, protecting pDNA and achieve endosome escape after entering cells. From Figure 7A and 7B, when the mass ratio of APCDs-OA conjugates to GFP plasmids was increased from 20:1 to 40:1, the green fluorescence signals also increased, demonstrating that the transfection efficiencies of APCDs-OA conjugates are dose-dependent.

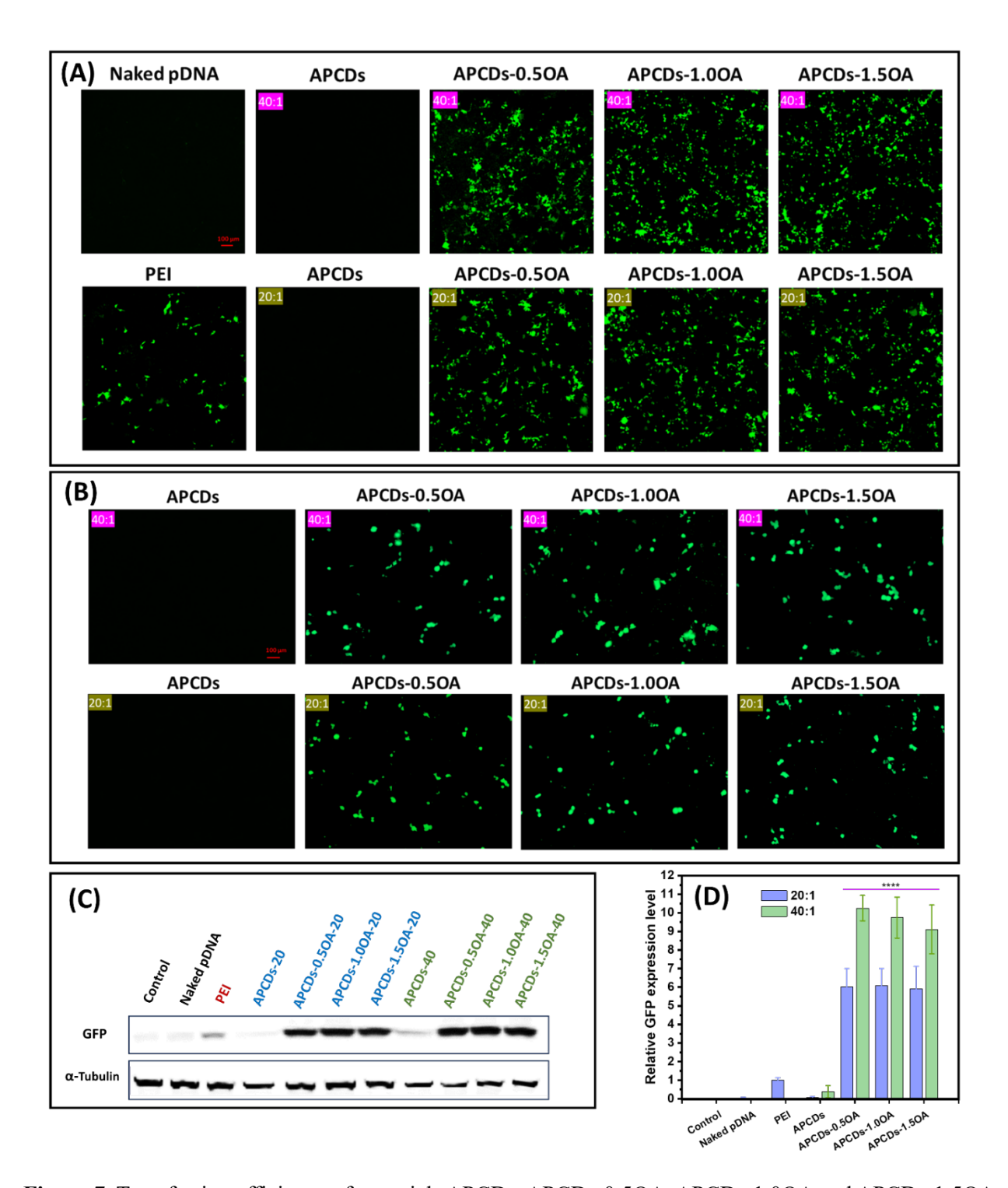


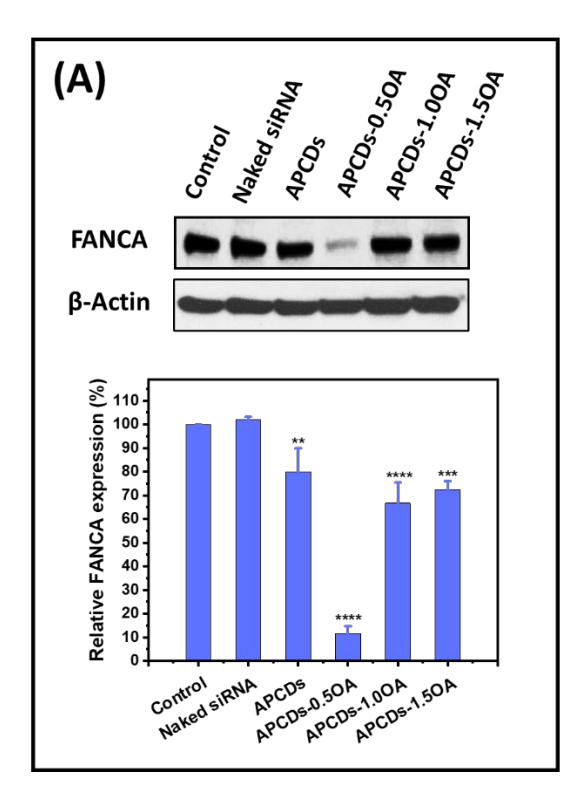
Figure 7. Transfection efficiency of materials APCDs, APCDs-0.5OA, APCDs-1.0OA and APCDs-1.5OA at different mass ratio of material to pDNA in (A) HEK 293 and (B) U2OS cells. The cells treated only with pDNA or pDNA with OA were used as negative controls, while the 25 kDa PEI with pDNA were used as positive controls. (C) Western blot analysis of GFP expression in HEK 293 cells. (D) Quantification of Western Blot results: relative GFP expression level of HEK 293 cells treated by varied materials. The GFP expression mediated by PEI were set as 1. Statistical significance is determined by using the one-way ANOVA analysis. *p<0.05, **p<0.01, ***p<0.001, ****p<0.0001, compared to PEI group.

To quantify GFP expression and determine the best pDNA delivery vehicle, Western blot analysis was performed. As shown in **Figure 7C**, GFP bands were not observed in cells treated only with pDNA or cells incubated with APCDs and pDNA, which matches the result in **Figure S4** and **7A**. Cells treated with pDNA using PEI, APCDs-0.5OA, APCDs-1.0OA and APCDs-1.5OA as carriers exhibit obvious GFP bands. From Figure **7D**, GFP expression level mediated by APCDs-0.5OA, APCDs-1.0OA and APCDs-1.5OA at the mass ratio of 20:1 is six times greater than that of PEI. As the mass ratio increased from 20:1 to 40:1, all APCDs-OA conjugates show increased and comparable GFP expression level, approximately nine or ten times higher than that of PEI. Besides the evaluation of GFP expression, the cell viability of HEK 293 and U2OS cells after being transfected with pDNA were detected. As the results shown in **Figure S9A-9B**, the cell viability of both types of cells are all higher than 80%. Therefore, the GFP plasmids delivery experiments above demonstrate that APCDs-OA conjugates are good vehicle candidates for pDNA delivery.

3.6 Delivery of siRNA

siRNA is a class of double-stranded RNA that can silence protein expression by targeting complementary mRNA for its cleavage and degradation. 53 It has been widely explored in therapeutics. 53 To evaluate the siRNA transfection efficiency of the synthesized APCDs and APCDs-OA conjugates, two siRNA for silencing FANCA and FANCD2 proteins which involved in DNA repair were selected as siRNA models. 54, 55 The expression levels of FANCA and FANCD2 proteins in U2OS cells were analyzed by Western blot. Regarding vehicles, the mass ratio of the as-prepared material to siRNA was 40:1. The cells without any treatment were set as control. The results in Figure 8 indicate that the expression of FANCA and FANCD2 proteins were not affected in cells treated with naked siRNA. The transfection efficiency of APCDs is negligible. Similar to the results in pDNA delivery, conjugation of OA to APCDs can improve the siRNA transfection efficiency of materials. As depicted in Figure 8A and 8B, APCDs-0.5OA show the highest siRNA delivery capability. With APCDs-0.5OA as carriers, the relative expression of FANCA and FANCD2 proteins were silenced from 100% to 9.9 % and 19.1 %, respectively, compared with the control. In comparison, the expressions of these two proteins were only silenced to 60 – 70 % in cells utilizing APCDs-1.0OA and APCDs-1.5OA as vehicles, inferring that excess OA on APCDs-OA conjugates is not beneficial in siRNA delivery. This phenomenon can be

explained by the fact that APCDs-1.0OA and APCDs-1.5OA have significantly lower siRNA binding ability than that of APCDs-0.5OA, which has been proved by agarose gel electrophoresis results in **Figure 2A**. The cell viability of U2OS cells was not affected after transfection (**Figure S10**). APCDs-0.5OA has potential to be an ideal vehicle for siRNA delivery.



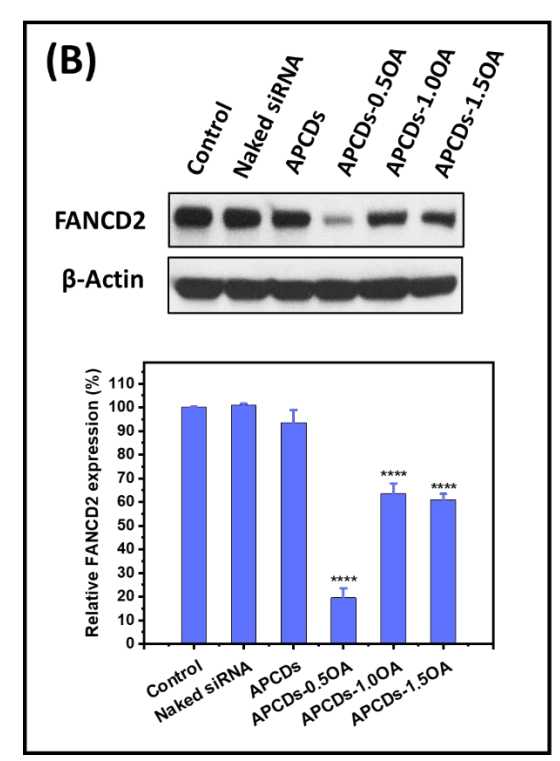


Figure 8. siRNA transfection efficiency of materials APCDs, APCDs-0.5OA, APCDs-1.0OA and APCDs-1.5OA in U2OS cells. Data are shown as mean \pm SEM. Statistical significance was determined by using the one-way ANOVA analysis. *p<0.05, **p<0.01, ***p<0.001, ***p<0.000, compared to control.

3.7 Intracellular trafficking

Since the efficient gene transfection ability of the as-prepared APCDs-OA conjugates has been proven, the intracellular trafficking of Cy3-siRNA and Cy3-DNA-based complexes formed by using APCDs-0.5OA as a carrier model at a mass ratio of 40:1 was determined in U2OS cells to investigate the delivery mechanism. After incubation for 1, 2 and 4 h with the complexes, the cell nucleus was stained with Hoechst 33342, while the endosomes were stained with LumiTracker Lyso green. The cells without the adding of complexes were set as controls. As shown in **Figure 9**, with cell incubation for 1 h, Cy3-siRNA signals were observed and overlapped with the green signals for endosomes, indicating that the Cy3-siRNA-based complexes were trapped in endosomes upon entering the cells. With the incubation time increasing from 1 to 2 and 4 h, some

Figure 9. Intracellular tracking of Cy3-siRNA loaded APCDs-0.5OA complexes in U2OS cells with different incubation time. The cell nucleus was stained by Hoechst 33342 (blue channel) and the endosomes were stained by LumiTracker Lyso green (green channel). The cells without Cy3-siRNA and APCDs-0.5OA were set as controls.

4. Conclusion

671672

673

674 675

676

677

678

679

680

681

668

669

670

In this project, the positively charged APCDs which were derived from Arg and PEHA as precursors were first synthesized and conjugated with OA for gene delivery applications. The asprepared APCDs possess a small size of 2 nm and exhibit excitation-dependent photoluminescence properties. By varying the mass ratio of APCDs to OA from 0.5:1 to 1:1 and 1.5:1, the obtained APCDs-OA conjugates including APCDs-0.5OA, APCDs-1.0OA and APCDs-1.5OA exhibit the

merits of amphiphilic structures. Confirming through agarose gel electrophoresis study, UV-vis 682 and fluorescence spectroscopies, taking advantages of positively charged APCDs and hydrophobic 683 684 oleoyl chain of OA, these APCDs-OA conjugates can bind with DNA via electrostatic interactions and form stable APCDs-OA conjugate-DNA complexes. The strong siRNA binding capability of 685 APCDs-0.5OA was also proved via agarose gel electrophoresis experiments. In addition, the 686 cellular uptake investigations in HEK 293 and U2OS cells demonstrate that all the APCDs and 687 APCDs-OA conjugates can efficiently penetrate the cell membrane and distribute in both the 688 cytoplasm and the nucleus which serve as active sites for siRNA and pDNA, respectively. 689 Evaluating via GFP pDNA delivery studies, all the prepared APCDs-OA conjugates show high 690 pDNA transfection efficiency in HEK 293 and U2OS cells, especially the transfection efficiencies 691 of APCDs-0.5OA and APCDs-1.0OA in HEK 293 cells are ten times greater than that of PEI. 692 693 Regarding siRNA delivery, after transfection of FANCA siRNA and FANCD2 siRNA into U2OS cells with APCDs-0.5OA as vehicles, the expression of FANCA and FANCD2 proteins were 694 695 downregulated to 9.9 and 19.1 %, respectively, indicating the excellent siRNA transfection efficacy of APCDs-0.5OA. Consequently, the gene delivery system in this study combines the advantages 696 697 of lipid structure and CCDs, significantly improving the transfection efficiency of carriers to both pDNA and siRNA. Based on the intracellular trafficking experiment, the delivery involves 698 699 endosomal escape mechanism. This study offers a strategy in the development of highly effective gene delivery vehicles. 700

Author information

- 702 Corresponding authors
- 703 Roger M. Leblanc Department of Chemistry, University of Miami, Coral Gables, FL 33146,
- 704 USA;

701

- 705 Email: rml@miami.edu
- Yanbin Zhang Department of Biochemistry and Molecular Biology, Miller School of Medicine,
- 707 University of Miami, FL 33136, USA;
- 708 Email: yzhang4@med.miami.edu

709 Author contributions

†Jiuyan Chen, Fang Li and Bowen Zhao contributed equally to this work.

712 Notes

713 The authors declare no competing financial interest.

714 Acknowledgments

- Professor Roger M. Leblanc thanks the support from the Florida Department of Health under grant
- GR022157. This work is also supported by the National Science Foundation CAREER award
- under grant No. 2238812 (F. Z.), National Institutes of Health under grant No. R01HL156958 (Y.
- 718 Z.), Department of Defense Prostate Cancer Research Program under grant No. PC200118 (F. Z.),
- and National Institutes of Health under grant No. R01GM129514 (F. Verde).

720 ASSOCIATED CONTENT

- 721 Supporting Information available. Additional characterizations related to APCDs and APCDs-OA
- 722 conjugates; zeta potential and TEM images of APCDs-pDNA and APCDs-OA conjugate-pDNA
- complexes; pDNA release from APCDs-pDNA and APCDs-OA conjugate-pDNA complexes; cell
- viabilities of HEK 293 and U2OS cells after transfection with pDNA and siRNA; intracellular
- 725 tracking of Cy3-DNA-APCDs-0.5OA complexes in U2OS cells.

726 References

- 1. Mendes, B. B.; Conniot, J.; Avital, A.; Yao, D.; Jiang, X.; Zhou, X.; Sharf-Pauker, N.;
- Xiao, Y.; Adir, O.; Liang, H.; Shi, J.; Schroeder, A.; Conde, J., Nanodelivery of nucleic acids.
- 729 *Nat. Rev. Methods Primers* **2022,** *2*, 1-21.
- Zuo, G.; Xie, A.; Pan, X.; Su, T.; Li, J.; Dong, W., Fluorine-doped cationic carbon dots
- 731 for efficient gene delivery. *ACS Appl. Nano Mater.* **2018,** *1* (5), 2376-2385.
- 732 3. Rezaei, A.; Hashemi, E., A pseudohomogeneous nanocarrier based on carbon quantum dots
- decorated with arginine as an efficient gene delivery vehicle. Sci. Rep. 2021, 11 (1), 13790, 1-10.
- 734 4. Dinis, T. B. V.; Sousa, F.; Freire, M. G., Insights on the DNA stability in aqueous solutions
- of ionic liquids. *Front. Bioeng. Biotechnol.* **2020**, *8*, 547857, 1-10.
- 736 5. Miron-Barroso, S.; Domenech, E. B.; Trigueros, S., Nanotechnology-based strategies to
- overcome current barriers in gene delivery. *Int. J. Mol. Sci.* **2021,** 22 (16), 1-18.
- 738 6. David, R. M.; Doherty, A. T., Viral Vectors: The road to reducing genotoxicity. *Toxicol. Sci.*
- **2017,** *155* (2), 315-325.

- 740 7. Wang, H.; Ding, S.; Zhang, Z.; Wang, L.; You, Y., Cationic micelle: a promising
- nanocarrier for gene delivery with high transfection efficiency. J. Genet. Med. 2019, 21 (7), e3101,
- 742 1-16.
- 743 8. Ma, K.; Mi, C. L.; Cao, X. X.; Wang, T. Y., Progress of cationic gene delivery reagents
- 744 for non-viral vector. *Appl. Microbiol. Biotechnol.* **2021**, *105* (2), 525-538.
- 745 9. Kargaard, A.; Sluijter, J. P. G.; Klumperman, B., Polymeric siRNA gene delivery-
- transfection efficiency versus cytotoxicity. *J. Controlled Release* **2019**, *316*, 263-291.
- 747 10. Wang, C.; Pan, C.; Yong, H.; Wang, F.; Bo, T.; Zhao, Y.; Ma, B.; He, W.; Li, M.,
- Emerging non-viral vectors for gene delivery. J. Nanobiotechnol. 2023, 21 (1), 272, 1-18.
- 749 11. Zare, H.; Ahmadi, S.; Ghasemi, A.; Ghanbari, M.; Rabiee, N.; Bagherzadeh, M.; Karimi,
- 750 M.; Webster, T. J.; Hamblin, M. R.; Mostafavi, E., Carbon nanotubes: smart drug/gene delivery
- 751 carriers. Int. J. Nanomed. **2021**, 16, 1681-1706.
- 752 12. Carvalho, A. M.; Cordeiro, R. A.; Faneca, H., Silica-based gene delivery systems: from
- design to the rapeutic applications. *Pharmaceutics* **2020**, *12* (7), 1-45.
- 754 13. Rai, R.; Alwani, S.; Badea, I., Polymeric nanoparticles in gene therapy: new avenues of
- design and optimization for delivery applications. *Polymers (Basel)* **2019,** *11* (4), 1-35.
- 756 14. Wang, B.; Song, H.; Qu, X.; Chang, J.; Yang, B.; Lu, S., Carbon dots as a new class of
- nanomedicines: opportunities and challenges. *Coord. Chem. Rev.* **2021,** *442,* 1-18.
- 758 15. Xu, D.; Lin, Q.; Chang, H. T., Recent advances and sensing applications of carbon dots.
- 759 *Small Methods* **2020,** *4* (4), 1-17.
- 760 16. Su, W.; Wu, H.; Xu, H.; Zhang, Y.; Li, Y.; Li, X.; Fan, L., Carbon dots: a booming
- material for biomedical applications. *Mater. Chem. Front.* **2020,** 4 (3), 821-836.
- 762 17. Zhou, Y.; Mintz, K. J.; Sharma, S. K.; Leblanc, R. M., Carbon dots: diverse preparation,
- application, and perspective in surface chemistry. *Langmuir* **2019**, *35* (28), 9115-9132.
- 764 18. Chen, J.; Li, F.; Gu, J.; Zhang, X.; Bartoli, M.; Domena, J. B.; Zhou, Y.; Zhang, W.;
- Paulino, V.; B, C. L. B. F.; Michael Brejcha, N.; Luo, L.; Arduino, C.; Verde, F.; Zhang, F.;
- Zhang, F.; Tagliaferro, A.; Olivier, J. H.; Zhang, Y.; Leblanc, R. M., Cancer cells inhibition by
- cationic carbon dots targeting the cellular nucleus. *J. Colloid Interface Sci.* **2023**, *637*, 193-206.
- 768 19. Yue, L.; Wei, Y.; Fan, J.; Chen, L.; Li, Q.; Du, J.; Yu, S.; Yang, Y., Research progress
- in the use of cationic carbon dots for the integration of cancer diagnosis with gene treatment. *New*
- 770 *Carbon Mater.* **2021,** *36* (2), 373-389.

- 771 20. Li, R.; Wei, F.; Wu, X.; Zhou, P.; Chen, Q.; Cen, Y.; Xu, G.; Cheng, X.; Zhang, A.;
- Hu, Q., PEI modified orange emissive carbon dots with excitation-independent fluorescence
- emission for cellular imaging and siRNA delivery. *Carbon* **2021**, *177*, 403-411.
- 774 21. Hasanzadeh, A.; Mofazzal Jahromi, M. A.; Abdoli, A.; Mohammad-Beigi, H.; Fatahi, Y.;
- Nourizadeh, H.; Zare, H.; Kiani, J.; Radmanesh, F.; Rabiee, N.; Jahani, M.; Mombeiny, R.;
- Karimi, M., Photoluminescent carbon quantum dot/poly-l-Lysine core-shell nanoparticles: a novel
- candidate for gene delivery. J. Drug Delivery Sci. Technol. 2021, 61, 1-7.
- 778 22. Hashemzadeh, I.; Hasanzadeh, A.; Radmanesh, F.; Khodadadi Chegeni, B.; Hosseini, E.
- 779 S.; Kiani, J.; Shahbazi, A.; Naseri, M.; Fatahi, Y.; Nourizadeh, H.; Kheiri Yeghaneh Azar, B.;
- Aref, A. R.; Liu, Y.; Hamblin, M. R.; Karimi, M., Polyethylenimine-functionalized carbon dots
- 781 for delivery of CRISPR/Cas9 complexes. ACS Appl. Bio Mater. **2021**, 4 (11), 7979-7992.
- 782 23. Hasanzadeh, A.; Radmanesh, F.; Hosseini, E. S.; Hashemzadeh, I.; Kiani, J.; Nourizadeh,
- 783 H.; Naseri, M.; Fatahi, Y.; Chegini, F.; Madjd, Z.; Beyzavi, A.; Kowalski, P. S.; Karimi, M.,
- 784 Highly photoluminescent nitrogen- and zinc-doped carbon dots for efficient delivery of
- 785 CRISPR/Cas9 and mRNA. *Bioconjugate Chem.* **2021**, *32* (8), 1875-1887.
- 786 24. Wang, Q.; Shi, L.; Zhao, J.; Shuang, S., Fluorescent carbon dots with real-time nucleolus-
- monitoring capability for gene delivery and biosensing of NO2- and pH. Appl. Surf. Sci. 2022,
- 788 *599*, 1-9.
- 789 25. Zhang, W.; Chen, J.; Gu, J.; Bartoli, M.; Domena, J. B.; Zhou, Y.; B, C. L. B. F.; Kirbas
- 790 Cilingir, E.; McGee, C. M.; Sampson, R.; Arduino, C.; Tagliaferro, A.; Leblanc, R. M., Nano-
- 791 carrier for gene delivery and bioimaging based on pentaetheylenehexamine modified carbon dots.
- 792 *J. Colloid Interface Sci.* **2023,** *639*, 180-192.
- 793 26. Liu, X.; Ma, D.; Tang, H.; Tan, L.; Xie, Q.; Zhang, Y.; Ma, M.; Yao, S., Polyamidoamine
- dendrimer and oleic acid-functionalized graphene as biocompatible and efficient gene delivery
- 795 vectors. ACS Appl. Mater. Interfaces **2014**, 6 (11), 8173-8183.
- 796 27. Chen, P.; Zhang, J.; He, X.; Liu, Y. H.; Yu, X. Q., Hydrophobically modified carbon dots
- as a multifunctional platform for serum-resistant gene delivery and cell imaging. *Biomater. Sci.*
- 798 **2020,** *8* (13), 3730-3740.
- 799 28. Salvador, C.; Andreozzi, P.; Romero, G.; Loinaz, I.; Dupin, D.; Moya, S. E., Self-
- 800 Assembled Oleic Acid-Modified Polyallylamines for Improved siRNA Transfection Efficiency
- and Lower Cytotoxicity. ACS Appl. Bio Mater. **2023**, 6 (2), 529-542.

- 802 29. Zhang, Y.; Sun, C.; Wang, C.; Jankovic, K. E.; Dong, Y., Lipids and Lipid Derivatives
- 803 for RNA Delivery. Chem. Review 2021, 121 (20), 12181-12277
- 804 30. Roda, A.; Santos, F.; Chua, Y. Z.; Kumar, A.; Do, H. T.; Paiva, A.; Duarte, A. R. C.;
- Held, C., Unravelling the nature of citric acid:L-arginine:water mixtures: the bifunctional role of
- 806 water. Phys. Chem. Chem. Phys. 2021, 23 (2), 1706-1717.
- 807 31. Estévez-Jácome, J.; Argáez, C.; Ramírez-Zamora, R.-M.; Alcántar-Vázquez, B., CO₂
- 808 adsorption on PEHA-functionalized geothermal silica waste: a kinetic study and quantum
- 809 chemistry approach. *React. Chem. Eng.* **2022**, 7 (9), 2025-2034.
- 810 32. Zhang, L.; He, R.; Gu, H., Oleic acid coating on the monodisperse magnetite nanoparticles.
- 811 Appl. Surf. Sci. **2006**, 253 (5), 2611-2617.
- 812 33. Bu, W.; Xu, X.; Wang, Z.; Jin, N.; Liu, L.; Liu, J.; Zhu, S.; Zhang, K.; Jelinek, R.;
- Zhou, D.; Sun, H.; Yang, B., Ascorbic acid-PEI carbon dots with osteogenic effects as miR-2861
- carriers to effectively enhance bone regeneration. ACS Appl. Mater. Interfaces 2020, 12 (45),
- 815 50287-50302.
- 816 34. Shu, M.; Gao, F.; Yu, C.; Zeng, M.; He, G.; Wu, Y.; Su, Y.; Hu, N.; Zhou, Z.; Yang,
- 817 Z.; Xu, L., Dual-targeted therapy in HER2-positive breast cancer cells with the combination of
- carbon dots/HER3 siRNA and trastuzumab. *Nanotechnology* **2020**, *31* (33), 335102, 1-12.
- 819 35. Luo, T.; He, X.; Zhang, J.; Chen, P.; Liu, Y.-H.; Wang, H.; Yu, X., Photoluminescent F-
- doped carbon dots prepared by ring-opening reaction for gene delivery and cell imaging. RSC Adv.
- **2018,** *8* (11), 6053-6062.
- 822 36. Zhou, Y.; Kandel, N.; Bartoli, M.; Serafim, L. F.; ElMetwally, A. E.; Falkenberg, S. M.;
- Paredes, X. E.; Nelson, C. J.; Smith, N.; Padovano, E.; Zhang, W.; Mintz, K. J.; Ferreira, B.;
- 824 Cilingir, E. K.; Chen, J.; Shah, S. K.; Prabhakar, R.; Tagliaferro, A.; Wang, C.; Leblanc, R. M.,
- Structure-activity relationship of carbon nitride dots in inhibiting tau aggregation. Carbon 2022,
- 826 *193*, 1-16.
- 827 37. Zhou, Y. Q.; Chen, J. Y.; Cilingir, E. K.; Zhang, W.; Gonzalez, L.; Perez, S.; Davila, A.;
- Brejcha, N.; Gu, J.; Shi, W. Q.; Domena, J. B.; Ferreira, B. C. L. B.; Zhang, F. W.; Vallejo, F.
- 829 A.; Toledo, D.; Liyanage, P. Y.; Graham, R. M.; Dallman, J.; Peng, Z. L.; Agatemor, C.;
- Catenazzi, A.; Leblanc, R. M., An insight into embryogenesis interruption by carbon nitride dots:
- can they be nucleobase analogs? *Nanoscale* **2022**, *14* (47), 17607-17624.

- 832 38. Wang, L.; Zhang, X.; Cui, Y.; Guo, X.; Chen, S.; Sun, H.; Gao, D.; Yang, Q.; Kang, J.,
- Polyethyleneimine-oleic acid micelle-stabilized gold nanoparticles for reduction of 4-nitrophenol
- with enhanced performance. *Transit. Met. Chem.* **2019**, 45 (1), 31-39.
- 835 39. Almeida, A.; Araujo, M.; Novoa-Carballal, R.; Andrade, F.; Goncalves, H.; Reis, R. L.;
- 836 Lucio, M.; Schwartz, S., Jr.; Sarmento, B., Novel amphiphilic chitosan micelles as carriers for
- 837 hydrophobic anticancer drugs. *Mater. Sci. Eng. C: Mater.* **2020,** *112*, 110920, 1-13.
- 838 40. Sabzehei, F.; Taromchi, A. H.; Danafar, H.; Rashidzadeh, H.; Ramazani, A., In vitro
- characterization of polyethyleneimine-oleic acid cationic micelle as a novel protein carrier. Adv.
- 840 Biomed. Res. 2023, 12, 126, 1-10.
- 841 41. Sahoo, D. K.; Jena, S.; Dutta, J.; Chakrabarty, S.; Biswal, H. S., Critical assessment of
- the interaction between DNA and choline amino acid ionic liquids: evidences of multimodal
- binding and stability enhancement. ACS Cent. Sci. 2018, 4 (12), 1642-1651.
- 844 42. Farghaly, T. A.; Abo Alnaja, A. M.; El-Ghamry, H. A.; Shaaban, M. R., Synthesis and
- DNA binding of novel bioactive thiazole derivatives pendent to N-phenylmorpholine moiety.
- 846 Bioorg. Chem. 2020, 102, 104103, 1-15.
- 847 43. Mansour, A. M.; Shehab, O. R., Lysozyme and DNA binding affinity of Pd(ii) and Pt(ii)
- complexes bearing charged N,N-pyridylbenzimidazole bidentate ligands. *Dalton Trans.* **2018**, 47
- 849 (10), 3459-3468.
- 850 44. Saswati; Mohanty, M.; Banerjee, A.; Biswal, S.; Horn, A., J.; Schenk, G.; Brzezinski,
- 851 K.; Sinn, E.; Reuter, H.; Dinda, R., Polynuclear zinc(II) complexes of thiosemicarbazone:
- synthesis, X-ray structure and biological evaluation. J. Inorg. Biochem. 2020, 203, 110908, 1-13.
- 853 45. Nie, Y.; Dai, Z.; Fozia; Zhao, G.; Jiang, J.; Xu, X.; Ying, M.; Wang, Y.; Hu, Z.; Xu,
- 854 H., Comparative studies on DNA-binding mechanisms between enantiomers of a polypyridyl
- ruthenium(II) complex. J. Phys. Chem. B. **2022**, 126 (26), 4787-4798.
- 856 46. Arif, R.; Rana, M.; Yasmeen, S.; Amaduddin; Khan, M. S.; Abid, M.; Khan, M. S.;
- 857 Rahisuddin, Facile synthesis of chalcone derivatives as antibacterial agents: synthesis, DNA
- binding, molecular docking, DFT and antioxidant studies. J. Mol. Struct. 2020, 1208, 1-13.
- 859 47. Shahabadi, N.; Zendehcheshm, S.; Khademi, F., Exploring the ct-DNA and plasmid DNA
- 860 binding affinity of the biogenic synthesized Chloroxine-conjugated silver nanoflowers:
- spectroscopic and gel electrophoresis methods. *Process Biochem.* **2022**, *121*, 360-370.

- 862 48. Shahabadi, N.; Zendehcheshm, S., Evaluation of ct-DNA and HSA binding propensity of
- antibacterial drug chloroxine: multi-spectroscopic analysis, atomic force microscopy and docking
- simulation. Spectrochim. Acta A Mo.l Biomol. Spectrosc. 2020, 230, 118042, 1-19.
- Aleksic, M. M.; Kapetanovic, V., An overview of the optical and electrochemical methods
- for detection of DNA drug interactions. *Acta Chim. Slov.* **2014**, *61* (3), 555-573.
- 867 50. Ottaviani, M. F.; Furini, F.; Casini, A.; Turro, N. J.; Jockusch, S.; Tomalia, D. A.; Messori,
- 868 L., Formation of supramolecular structures between DNA and starburst dendrimers studied by EPR,
- 869 CD, UV, and melting profiles. *Macromolecules* **2000**, *33* (21), 7842-7851.
- 870 51. Suzuki, I. L.; de Araujo, M. M.; Bagnato, V. S.; Bentley, M., TNFalpha siRNA delivery
- by nanoparticles and photochemical internalization for psoriasis topical therapy. J. Controlled
- 872 *Release* **2021,** *338*, 316-329.
- 873 52. Tezgel, Ö.; DiStasio, N.; Laghezza-Masci, V.; Taddei, A. R.; Szarpak-Jankowska, A.;
- Auzély-Velty, R.; Navarro, F. P.; Texier, I., Collagen scaffold-mediated delivery of NLC/siRNA
- as wound healing materials. J. Drug Delivery Sci. Technol. 2020, 55, 1-8.
- 876 53. Dana, H.; Chalbatani, G. M.; Mahmoodzadeh, H.; Karimloo, R.; Rezaiean, O.;
- 877 Moradzadeh, A.; Mehmandoost, N.; Moazzen, F.; Mazraeh, A.; Marmari, V.; Ebrahimi, M.;
- 878 Rashno, M. M.; Abadi, S. J.; Gharagouzlo, E., Molecular mechanisms and biological functions of
- 879 siRNA. J. Biomed. Sci. 2017, 13 (2), 48-57.
- 880 54. Benitez, A.; Liu, W.; Palovcak, A.; Wang, G.; Moon, J.; An, K.; Kim, A.; Zheng, K.;
- Zhang, Y.; Bai, F.; Mazin, A. V.; Pei, X. H.; Yuan, F.; Zhang, Y., FANCA Promotes DNA Double-
- Strand Break Repair by Catalyzing Single-Strand Annealing and Strand Exchange. *Mol. Cell* 2018,
- 883 71 (4), 621-628 e4, 1-20.

886

- 884 55. Palovcak, A.; Liu, W.; Yuan, F.; Zhang, Y., Stitching up broken DNA ends by FANCA.
- 885 *Mol. Cell. Oncol.* 2018, 5 (6), e1518101, 1-3.